Lamellar magnetism and exchange bias in billion-year-old metamorphic titanohematite with nanoscale ilmenite exsolution lamellae – III. Atomic-magnetic basis for experimental results

Peter Robinson,[1,*] S. A. McEnroe [2] R. J. Harrison,[2,3] K. Fabian [1,2] F. Heidelbach[4] and M. Jackson[5]

[1]*Geological Survey of Norway, N-7491 Trondheim, Norway*
[2]*Norwegian University of Science and Technology, N-7491, Trondheim, Norway. E-mail: suzanne.mcenroe@ntnu.no*
[3]*Department of Geosciences, Cambridge University, Downing St, Cambridge CB2 3EQ, UK*
[4]*Bayerisches Geoinstut, Universität Bayreuth, D95440 Bayreuth, Germany*
[5]*Institute of Rock Magnetism, University of Minnesota, Minneapolis, MN 55455, USA*

SUMMARY

Lamellar magnetism is a source of remanent magnetization in natural rocks different from common bulk magnetic moments in ferrimagnetic minerals. It has been found to be a source for a wide class of magnetic anomalies with extremely high Koenigsberger ratio. Its physical origin are uncompensated interface moments in contact layers of nanoscale ilmenite lamellae inside an hematite host, which also generate unusual low-temperature (low-*T*) magnetic properties, such as shifted low-*T* hysteresis loops due to exchange bias.

The atomic-magnetic basis for the exchange bias discovered in the hematite-ilmenite system is explored in a series of papers. In this third article of the series, simple models are developed for lamellae interactions of different structures when samples are either cooled in zero-field, or field-cooled in 5 T to temperatures below the ordering temperature of ilmenite. These models are built on the low-temperature measurements described earlier in Paper II. The important observations include: (i) the effects of lamellar shapes on magnetic coupling, (ii) the high-*T* acquisition of lamellar magnetism and low-*T* acquisition of magnetization of ilmenite lamellae, (iii) the intensity of lamellar magnetism and the consequent ilmenite magnetism in populations of randomly oriented crystals, (iv) lattice-preferred orientation of the titanohematite host crystal populations and (v) the effects of magnetic domain walls in the host on hysteresis properties. Based on exemplary growth models of lamellae with different geometries and surface couplings we here provide simple models to assess and explain the different observations listed above. Already the simplified models show that the shapes of the edges of ilmenite lamellae against their hematite hosts can control the degree of low-*T* coupling between ilmenite, and the lamellar magnetic moments. The models also explain certain features of the low-*T* exchange bias in the natural samples and emphasize the role of lattice-preferred orientation upon the intensity of remanent magnetization. The inverse link between ilmenite remanence and exchange-bias shift in bimodal low-*T* ilmenite lamellae is related to different densities of hematite domain walls induced by the clusters of ilmenite lamellae.

Key words: Magnetic properties; Microstructure; Magnetic mineralogy and petrology; Rock and mineral magnetism.

* deceased

1 INTRODUCTION

The 1 billion-yr-old natural remanent magnetization (NRM) of metamorphic rocks from Modum, Norway, creates magnetic exchange bias when cooled in zero field below the ordering temperature of ilmenite (McEnroe *et al.* 2007; Fabian *et al.* 2008). In two preceding papers (McEnroe *et al.* 2016; Robinson *et al.* 2016), here referred to respectively as Papers I and II, we studied mineralogy, rock magnetism and NRM-induced exchange bias of a new set of samples (MOD22) from the Modum area. In this third paper, we provide a physical interpretation of the hysteresis loops run at 5 K in fields up to 5 Tesla (T). The foundation of this study is the recent improvement in our understanding of the hematite–ilmenite phase diagram and its consequences for exsolution and resultant phase compositions in the entire temperature range from 950 to 5 K (Robinson *et al.* 2002, 2004). A physical explanation of the magnetic behaviour requires an understanding of lamellar magnetism and coupled ilmenite magnetism at several levels: (i) at the level of individual ilmenite lamellae in a hematite host, and their nature resulting from arrested lamellar growth during cooling from high-temperature regional metamorphism; (ii) at the level of clusters of lamellae within a single crystal, and how the magnetic properties of crystals may be controlled by their orientation with respect to the magnetizing field at the time of exsolution and (iii) at the level of populations of crystals containing such magnetized clusters within rock samples, either with a random orientation distribution or with lattice-preferred crystal orientations with respect to the magnetizing field at the time lamellar magnetism was created during exsolution. Also of crucial importance, as emphasized in Paper II, is the orientation of the NRM of each sample within the Magnetic Properties Measurement System (MPMS).

2 KEY FEATURES FROM HYSTERESIS EXPERIMENTS

Here we summarize the main features of the low-T exchange bias in ilmeno-hematite hysteresis loops as presented in Paper II. A remarkable feature observed after zero-field cooling of the NRM to 5 K, is that the hysteresis loops are bimodal. The difference $\Delta M(H)$ between upper and lower branches of the loops has two asymmetric peaks, one in positive field, and one in negative field. If the lamellar NRM vector measured at room temperature (RT) before the experiment is oriented towards the positive field direction ($+Z$) in the MPMS, then the larger $\Delta M(H)$ occurs in a negative field, and likewise NRM oriented towards $-Z$ results in a dominant $\Delta M(H)$ peak in a positive field. When the same samples are cooled in a field of $+5$ T from RT to 5 K before the hysteresis experiment, $\Delta M(H)$ has a unimodal peak at negative fields. These experiments, and the vanishing of exchange bias above T_N (McEnroe *et al.* 2007; Fabian *et al.* 2008), suggest that the conditions under which the samples were cooled below T_N of ilmenite, and thus acquired an ilmenite remanent magnetism coupled to the room-T lamellar magnetism, are critical in determining the nature and degree of the exchange bias (Harrison *et al.* 2007). This indicates that the exchange coupling to the high anisotropy of low-T ilmenite magnetism is responsible for the exchange bias, which agrees with quantitative models (Shcherbakov *et al.* 2009). This link between RT NRM and LT exchange bias proves that the same magnetic units that create the exchange coupling at the hematite–ilmenite interfaces also carry the NRM (Fabian *et al.* 2008).

To quantify correctly the exchange bias by hysteresis parameters, one has to avoid definitions of the bias field H_{EB}, which are purely based on coercivity or remanence, as clarified in Fig. 1. The hysteresis curves measured here, are composed of a biased ferrimagnetic loop (Hys_1 in Fig. 1a) and an anhysteretic loop (blue in Fig. 1) that represent the paramagnetic or diamagnetic minerals in the sample together with any anhysteretic parts of the magnetically ordered fraction. The sum of these parts (red loop in Fig. 1) is a biased loop with asymmetric coercivities H_c^+ and H_c^-, and asymmetric remanent magnetizations M_r^+ and M_r^-. Unfortunately, as Fig. 1(b) illustrates, the same, or very similar, asymmetries in H_c and M_r can be achieved without any exchange coupling, if the sample contains a magnetized fraction that vertically offsets the ferrimagnetic loop (Hys_2 in Fig. 1b), and that cannot be remagnetized in the applied field range. These two types of asymmetry can be clearly distinguished by the symmetry of $\Delta M(H)$, which is shifted only in case of true exchange bias. If $\Delta M(H)$ is unimodal, the exchange-bias field H_{EB} can be defined either as the position of the mode of $\Delta M(H)$, or by the center-of-mass of the total area of $\Delta M(H)$ (McEnroe *et al.* 2007; Fabian *et al.* 2008). For bimodal loops, the shift of each mode has to be estimated separately. By two different measures, the hysteresis shifts are consistently much larger for the bimodal loops (up to 1.68 T), than for the unimodal loops (<0.7 T). In addition, among the bimodal loops, the shift is generally larger for the side of the loop with the smaller opening than for the side with the larger opening. Another feature of the bimodal loops, as portrayed in graphs of $\Delta M(H)$, is that each mode individually is asymmetric, almost all with shallower slopes towards higher fields and steeper slopes towards lower fields. The effect of this is that hysteresis shifts measured by peak separation height are generally smaller, than shifts measured by peak centre-of-mass. A negative orientation of the NRM sample vector in the MPMS always leads to a larger $\Delta M(H)$ in a positive field, and vice versa. Aside from this, the actual angle between NRM and MPMS measurement direction has less control on the relative size of the two modes of $\Delta M(H)$. Using the graphs of $\Delta M(H)$, we express this relative mode height as the ratio of the larger peak-height to the sum of the peak-heights of both openings, B_{pk}/B_{Total}, whereby negative values indicate that the largest peak occurs at negative field values (Table 1). No values exceed 73 per cent, and most are close to 50 per cent. Although the exact placement angle seems unimportant, the intensity of RT NRM, as measured in the MPMS axis direction (NRM$_Z$), appears important. The four samples with the largest deviations from 50 per cent are also the four with the largest NRM$_Z$ intensities. These features require investigation. Despite the asymmetry of the hysteresis loops in intermediate fields, the intercepts of the loops at $+5$ T and -5 T are symmetrical, which means that $M(-5\,T) = -M(5\,T)$. This symmetry of the loops at high fields suggests that the lamellar magnetism is switched below these fields, overcoming the existing antiferromagnetic (AF) coupling with the adjacent ilmenite. An additional 'remanence shift', as in Fig. 1(b), which would indicate a strong ilmenite remanence, is not detectable. Despite this, the ilmenite remanence with high magnetocrystalline anisotropy obviously controls the features in the loop interiors. Several experimental observations suggest that the ilmenite remanence is little affected by fields to 5 T. For example, field-cooling curves presented in Paper II show that ilmenite acquires a negative remanence below T_N in a $+5$ T field (Robinson *et al.* 2016). This indicates that local AF coupling with the positive lamellar moments completely overcomes the effect of the $+5$ T field on the ilmenite magnetization. Such behaviour is in agreement with the observation that the metamagnetic transition into a ferromagnetic state requires
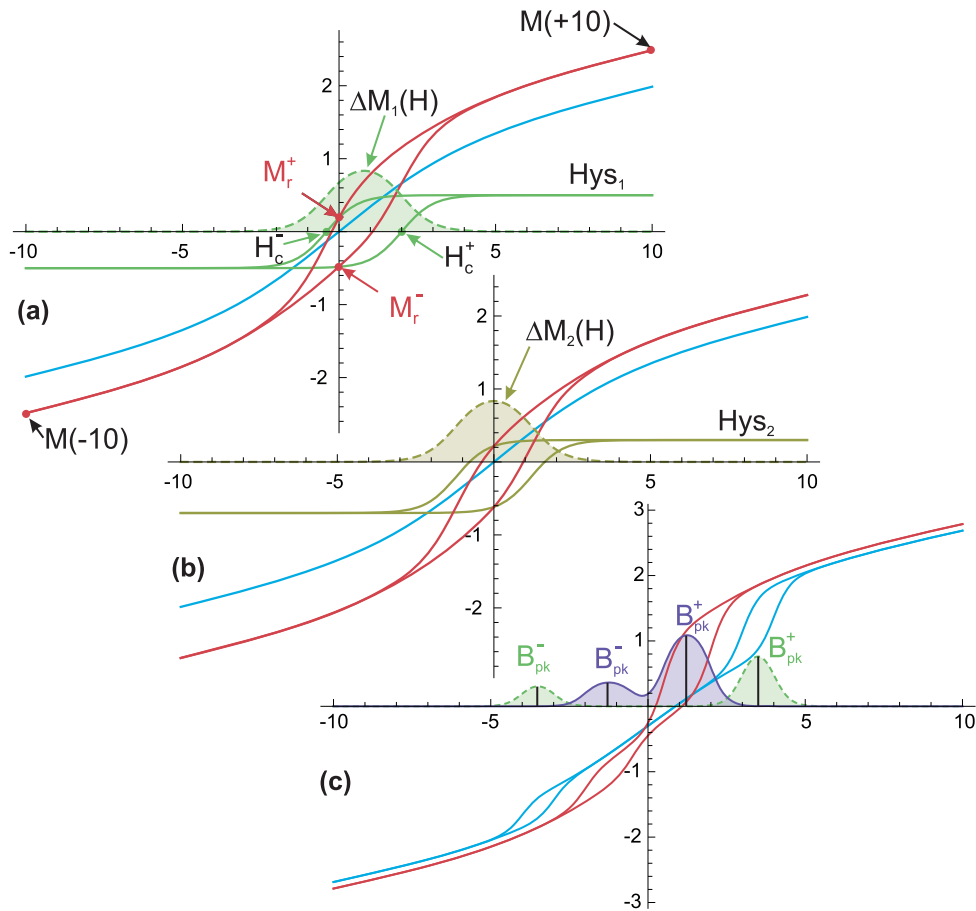
Figure 1. Terminology for shifted hysteresis loops. (a, b) the red hysteresis curve in both panels is the sum of a saturated hysteresis curve (green) and an anhysteretic curve (blue). The hysteresis difference (dashed) is the same for the green and the red hysteresis loops. (a) The saturated loop Hys_1 shows true exchange bias in that it is horizontally shifted by the bias field H_{EB}, whereby the coercive fields H_c^+ and H_c^- become asymmetric. The shift also breaks the symmetry of M_r^+ and M_r^-, such that their sum is not zero. True exchange bias also shifts the hysteresis difference ΔM_1 by the amount H_{EB}. This shift is not influenced by any anhysteretic curve (blue) added to Hys_1. (b) Remanence shift mimicking exchange bias occurs if the green curve is offset vertically, for example due to a unsaturated additional magnetic phase. The red curve also appears shifted in terms of asymmetric coercive fields H_c^+ and H_c^- and remanent magnetizations M_r^+ and M_r^-. The hysteresis difference remains symmetric in this case and can be used to distinguish true from mimicked exchange bias. (C) Hysteresis loops of exchange biased material where bias occurs in both directions. In the blue curve the bias fields are larger than the spread in coercivities, leading to two clearly separated peaks in ΔM (green). The red curve results from two populations of exchange bias that partly overlap leading to a bimodal ΔM (violet). Modal peak heights for negative and positive fields are denoted by B_{pk}^-, and B_{pk}^+, respectively.

Table 1. The measured ratios $M_{r,AV}$ (5 K)/NRM_Z(300 K) and B_{pk}/B_{Tot} (5K) compared to three lamellar models. Negative values of B_{pk}/B_{Tot} indicate that the maximal peak occurs at negative field values. Asterisks ($*$) indicate poor correlation between $M_{r,AV}$(5 K)/NRM_Z and B_{pk}/B_{Tot}. The last three column headers denote results from lamella models: μ_{Ilm} is the total low-T ilmenite moment in units of μ_B; ρ is the ratio of net low-T ilmenite moment/total lamellar moment and c_{CL} is the ratio of coupled contact layer surface area/total contact layer surface area.

Specimen	$M_{r,AV}$	NRM_Z	$M_{r,AV}/NRM_Z$	B_{pk}/B_{Tot}	μ_{Ilm}	ρ	c_{CL}
Fig. 5c					10717.6	0.658	0.822
I	+0.00351	+0.00428	0.820	−0.573∗			
C	−0.00594	−0.00782	0.760	+0.575∗			
F	+0.00664	+0.00914	0.726	−0.592∗			
G	+0.02443	+0.03390	0.721	−0.731			
A	−0.01153	−0.01730	0.667	+0.688			
Fig. 5a					7023	0.5	0.625
E	−0.00935	−0.01560	0.599	+0.593			
B	−0.00316	−0.00530	0.592	+0.538			
H	+0.00023	+0.000399	0.578	−0.568			
D	−0.00361	−0.00628	0.576	+0.536			
J	+0.00186	+0.00355	0.525	−0.552			
Fig. 5b					3758.8	0.380	0.465

Graphic Correlation Trend 0.6935.

a field in excess of 10 T (Kato *et al.* 1982). A similar effect was seen in experiments where the sample NRM vector was placed towards the negative field of the MPMS before cooling to 5 K, producing a positive ilmenite remanence. After a +5 T NRM hysteresis loop was measured, the field was switched to zero, the mean remanence, $M_{r,AV}$, was consistently negative (Robinson *et al.* 2016, Table 5). An earlier investigation in Robinson *et al.* (2016, fig. 5) showed a remarkable correlation between the intensity of the component of lamellar magnetism oriented in the direction of the MPMS (NRM_Z) and the resultant average moment in the loop at 5 K in zero field ($M_{r, AV}$) of the upper (M_r^+) and lower (M_r^-) limbs. The mean correlation coefficient for all values, both positive and negative is 0.69, with individual values from 0.58 to 0.82 (their Table 7, Table 1 here). Likely this coefficient is related to the total amount of AF coupling between lamellar moments and the ilmenite moments at 5 K. Logically this could be tied to details of magnetic coupling along the surfaces of individual ilmenite lamellae, which have local shape differences, though similar on average.

3 ATOMIC AND MAGNETIC DETAILS OF NANOSCALE EXSOLUTION LAMELLAE

Beyond understanding the general mechanism by which lamellar magnetism is acquired, it is crucial to understand the results of how ilmenite lamellae grow in a hematite host, and what atomic features in and around them are important in acquisition of lamellar magnetism at high *T*, and in acquisition of ilmenite magnetization at very low *T*. In the MOD22 samples, the ilmenite lamellae identified in TEM are commonly 1.2–1.7 nm thick, 12.5–17 nm long in section, and have aspect ratios between 7 and 13 (McEnroe *et al.* 2016), though smaller and scarce larger lamellae may be present. Hematite lamellae were not observed in the ilmenite lamellae. The approximate thickness of an atomic layer parallel to (001) in rhombohedral oxide is ≈0.23 nm. A lamella with two Ti layers and one internal Fe^{2+} layer is 0.69 nm thick, with 3 Ti layers and 2 Fe^{2+} layers is 1.15 nm thick, and with 4 Ti layers and 3 Fe^{2+} layers is 1.61 nm thick. The Monte Carlo simulations of Harrison *et al.* (2007) showed magnetic exchange bias works effectively only in lamellae with an odd number of Fe^{2+} layers and a net ilmenite moment, here at thicknesses of 0.69 and 1.61 nm. Information on thickness and aspect ratio is used to make models of lamellar shapes produced by different modes of growth. In contrast to synthetic crystallites of individual hematite nanoparticles (Sharma *et al.* 2018), we do not assume size dependent contraction or expansion of the lattice parameters in the natural lamellar system. Different shapes have consequences for the relative values of magnetic moments of lamellar magnetism at room *T*, and for the magnetic moments of ilmenite magnetism below 57 K.

3.1 Lamellar disks, cationic populations, magnetic moments and effects of varied disk radii

A simplified concept of ilmenite lamellae is that they are approximately circular flat disks parallel to (001) that grew first with a single layer Ti layer, then with a second layer added on the top, a third layer on the bottom, and then a fourth layer on the top again (Fig. 2). The top view Fig. 2 shows layers 1, 2 and 4, the centre view a vertical slice normal to (001), and the bottom view shows layers 1 and 3. An important aspect, critical to later interpretation, is that the total interface area of the contact layer (pink) depends only on
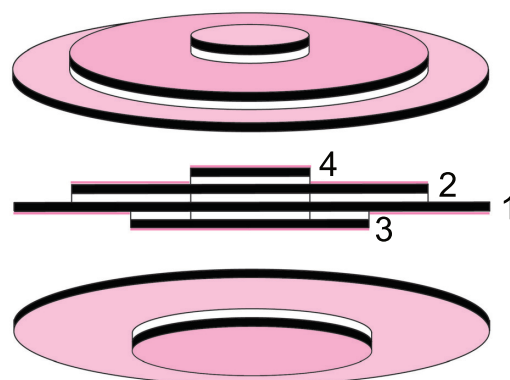

Figure 2. Idealized views of an ilmenite lamella within a hematite host. Black indicates Ti^{4+} layers, white indicates Fe^{2+} layers in ilmenite, which are paramagnetic above T_N. Pink surfaces show the positions of contact layers magnetized during lamellar growth. During growth at $T \gg T_N$ the four disk-shaped layers exsolved sequentially in four steps indicated by the numbers. In a positive field (e.g. to right) this results in a lamellar magnetic remanence that is positive or negative, depending on the position of the layers with respect to the hematite host. Only below T_N do the interior Fe^{2+} layers become magnetized.

the largest disk radius (layer 1 in Fig 2), and not on the number of stacked disks, or the radii of the smaller disks. The physical stepped-growth process is controlled and eventually terminated by the need to gather Ti and Fe^{2+} from the surrounding host from increasingly greater distances during a period of falling temperature, with the additional hindrance of increased lattice strain from insertion of large ilmenite into a smaller hematite host. We show that with different models of lamellae, growth style can control lamellar shape, which in turn controls the degree of magnetic coupling between lamellar contact layers and internal ilmenite Fe^{2+} layers mainly after cooling below T_N of ilmenite (Robinson *et al.* 2004; Harrison *et al.* 2007).

Fig. 3 provides a more complete picture of the ionic occupations of the cation layers. Each hexagonal plate contains one cation in the center, one cation at each of three corners, each 1/3 within the cell, and three vacancies at the other three corners, again each only 1/3 within the cell. Two rectangles cut across each hexagonal plate, and bisect the angle between the a_1 and a_2 crystallographic axes. These rectangles represent the diagonal vertical plane, with indices (1 1–2 0). It contains the 30° tilted 300 K magnetic moments of hematite (Fig. 3a) and contact layers (Figs 3b and c), and also the low-T magnetic moment of an ilmenite Fe^{2+} layer (Fig. 3e). Each pair of vertical rectangles represents the locations of two cations contained within a hexagonal plate one atomic layer thick parallel to (001) and having the footprint on (001) of a single hexagonal unit cell. These same rectangles will be used in later vertical slice figures through a lamella to portray the locations of cations and the orientations of their magnetic moments. Each cation layer is an assemblage of such hexagonal plates. Fig. 3 shows that there are five types of hexagonal plates (A–E) within hematite containing ilmenite exsolution lamellae. Plates A are composed mainly of Fe^{3+} cations in hematite layers. These are shown with their magnetic moments tilted upward 30° out of the (001) plane. The thickness of a hematite plate is 2.291Å and its diameter along the plane (1 1–2 0) is 5.81Å. Plates B and C are hybrid contact layers composed of equal numbers of Fe^{3+} and Fe^{2+} cations. Plate B shows a contact layer that would be 'on top' of a Ti layer. Here the Fe^{2+} cation is 'puckered' downward
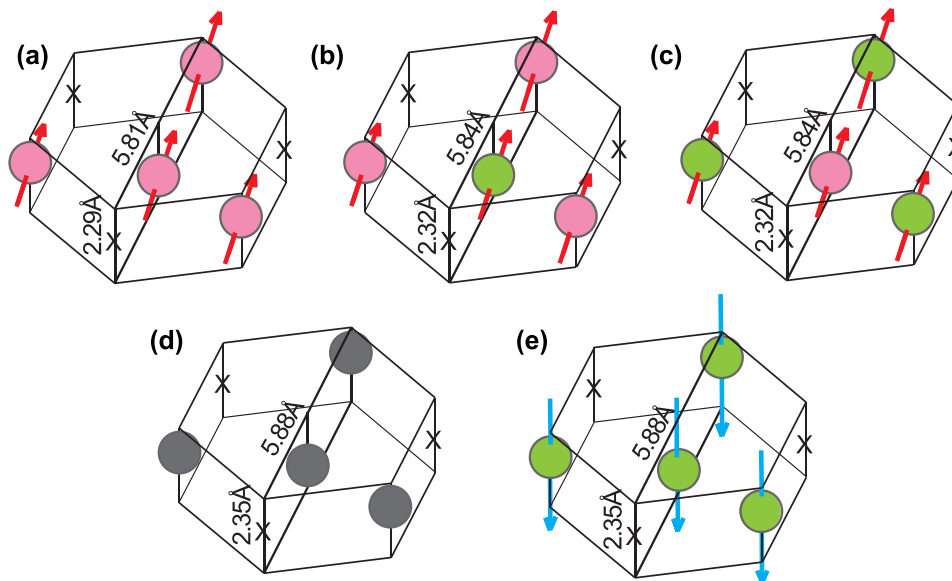
Figure 3. Images of the five types of cationic hexagonal plates with the footprint of a hexagonal unit cell on (001) in rhombohedral oxide. Colours indicate cation type, Fe^{3+}: pink, Fe^{2+}: green, Ti^{4+}: grey. Layer thicknesses in Å: 2.29 for hematite (a), 2.35 for ilmenite (d, e), and an estimated average 2.32 for contact layers (b, c). length of hexagon diagonals in å: 5.81 (a), 5.84 (b, c), 5.88 (d, e). Making a 'unit' cell of these hexagonal plates requires shifting cations for correct stacking sequence, but the number of 2 cations per plate is constant.

towards the Ti layer consistent with Monte Carlo simulations (Harrison *et al.* 2007), bond valence (Robinson *et al.* 2006b) and DFT calculations (Pentcheva & Nabi 2008). Plate C shows a contact layer that would be 'below' a Ti layer. Here the Fe^{2+} cations are 'puckered' upward towards the Ti layer. Present evidence suggests that the magnetic moments at the exsolution temperature, and at room temperature, would have essentially the same upward tilt as those in the hematite layer. Contact layer plates should have dimensions intermediate between those of hematite and those of ilmenite, with a probable thickness of 2.32Å and diameter 5.84 Å. Plate D shows the positions of Ti ions in ilmenite and Plate E shows positions of Fe^{2+} cations in ilmenite. The Ti^{4+} cations have no unpaired spins and are thus diamagnetic. The Fe^{2+} cations are shown with their magnetic moments below the 57 K Néel temperature oriented downward at an angle of 90° to (001) and thus AF coupled to the upward vertical component of the contact layers in plates B and C. Ilmenite plates should have average thickness 2.35Å and diameter 5.88Å.

The cationic disks in the oxide host and lamellae are essentially assemblages of the hexagonal plates of Fig. 3 where the diameters and radii of the disks are measured along the diagonal of the plates. Many such hexagonal plates form the quasi-circular disks that make up a lamella within the hematite host. The distribution of cations in such a layer, here a B contact layer, is shown in Fig. 4. A single slice through a lamella along a Ti layer must show an integral number of cations, so real fractional radii are not possible in two dimensions. However, particularly for lamellae with large radius, minor irregularities provide the possibility to have an integral number of atoms in a layer, represented by a non-integral value of layer radius. Thus, we justify the use of fractional radii to calculate lamellar areas and volumes, cation occupations and resultant magnetic properties.

3.2 The strong anisotropy of ilmenite magnetization in lamellae

In addition to the strong intralayer FM interaction in ilmenite, there is the interlayer AF interaction between two ilmenite Fe^{2+} layers
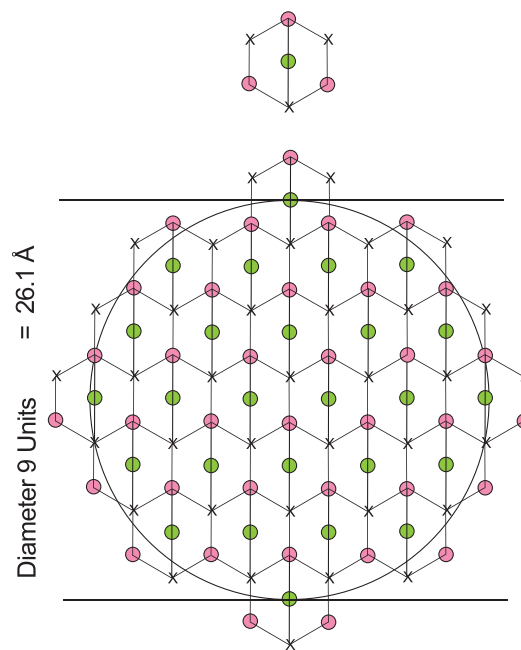

Figure 4. View of cation positions of a contact layer (Fig. 3b) on (001) compared to a cationic disk of radius 4.5 units and diameter 9 units (26.1 Å) with calculated area 63.62 units. The area of a hexagon with 2 cations is $3/2\sqrt{3}$, so the theoretical number of cations in the disk is 48.97, compared to a visual count of ≈48.8 cations.

that keeps their magnetic moments opposite. This interaction is important in the parts of a lamella with more than one Fe^{2+} layer, and stabilizes the ilmenite moments, once set. The single-ion anisotropy of Fe^{2+} in ilmenite (Kato *et al.* 1982) holds the magnetic moments normal to the layers even without interlayer interaction. With this anisotropy, then, the thin edges of the lamella would be just as involved in exchange bias as the thicker center. Also, then, it would

be possible to have magnetic exchange bias created by lamellae with only a single Fe^{2+} layer.

Key factors affecting the exchange coupling between hematite host and ilmenite lamellae are summarized in Fig. 5. Possible spin structures adopted below the ilmenite $T_N = 57$ K are illustrated for three different ilmenite growth models. The hematite host is shown with spins oriented at an angle $\sim 30°$ to the (001) basal plane. Ilmenite spins are oriented along [001]. Experimental results indicate that the low-T ilmenite magnetizations are very hard and possibly not shifted in a field of 5 T (see Fig. 1). Fundamentally, this results from the strong magnetic anisotropy of Fe^{2+} coordinated to six oxygens (Kato *et al.* 1982). Further strengthening can be understood by examining the ilmenite magnetizations in the growth step model of Fig. 2. During growth Step I, an ilmenite lamella would have only one Ti layer and no ilmenite moments, hence could only show magnetism below the blocking T of the hematite host (see cells 16.3–22 in Fig. 5b). In growth step II, an ilmenite lamella has two Ti layers and one internal Fe^{2+} layer with an ilmenite moment AF coupled to the lamellar moment on both sides (see cells 10.1–16.3 in Fig. 5b). The next-nearest-neighbour-interlayer coupling between the lamellar moment of the contact layers and the ilmenite moment is relatively weak. However, once this AF coupling has determined the direction of the ilmenite moment on cooling, the single Fe^{2+} ion anisotropy of ilmenite will fix the moment even in a strong field of up to 5 T. The situation after growth step II is the earliest situation where there are two internal Fe^{2+} layers in the ilmenite (see cells 4.5–10.1 in Fig. 5b). This is then the first opportunity for the relatively weak AF interactions between the two layers support the anisotropy, in addition to the strong FM interaction along the layers that force the entire ilmenite Fe^{2+} layers into the same magnetic orientation. The second added Fe^{2+} layer acquires a positive moment opposite to the negative moment of the original Fe^{2+} layer, partly frustrating the strong intralayer interaction. Growth step IV adds another ilmenite Fe^{2+} layer, further enhancing the antiferromagnetic interactions between Fe^{2+} layers, and also adding still more positive ilmenite moments to the total (see cells 0–4.5 in Fig. 5b). However, that positive total, for these models, is still less than the total of negative ilmenite moments. The general concept here is that the weak AF interactions between Fe^{2+} layers in the thicker parts of the lamella help retain the orientations of the magnetic moments in high fields, but these orientations are also maintained by single-ion anisotropy in the thin edge, where those weak interactions are absent.

Below T_N, for some Fe^{2+} spins it is impossible to align with the exchange forces from all neighbours. Local belt-shaped areas of frustrated intralayer interactions develop within the Fe^{2+} layers (highlighted in violet in Fig. 5). Yet, in all lamellar models with a positive lamellar magnetic moment carried by contact layers at high T, a dominant negative ilmenite moment will result at low T. This dominance of negative ilmenite moments is expressed by the values of Negative Ilm Moment/Total Ilm Moment >0.5 reported in Fig. 5.

3.3 Possible source of strong correlation between NRM_Z at 300 K and $M_{r,\,AV}$ at 5 K

For biased hysteresis loops the average remanence can be defined by

$$M_{r,AV} = \frac{M_r^+ + M_r^-}{2},$$

where M_r^+ and M_r^- are the remanent magnetizations after positive and negative maximum applied fields (Fig. 1a). For symmetrical loops, the value of $M_{r,AV}$ is zero.

Fig. 5 and Table 7 in Paper II report a remarkable correlation between the orientation of the NRM vector in the MPMS z-direction (NRM_Z) at 300 K and the value of $M_{r,AV}$ at 5 K. For convenience, the experimental data from Paper II are also included in Table 1.

This observed relation between $M_{r,AV}$ and NRM_Z indicates that the samples still 'remember' the billion-year-old field in which the lamellae formed, even while undergoing a 5-Tesla loop at low T. This relates to the total effect of the ilmenite remanence on AF coupling between contact layers, and ilmenite Fe^{2+} layers at low T in a large population of variously oriented crystals. Table 1 compares three lamellar growth models with respect to their total moment of magnetized ilmenite layers μ_{Ilm}, and the ratio

$$\rho = \frac{\mu_{Ilm}}{\mu_{Lam}},$$

where μ_{Lam} is the corresponding lamellar moment.

The absolute value of the net ilmenite moment is smaller than the contact layer moment, which depends only on the contact layer surface area of the lamella. The net ilmenite moment of the lamella depends on the details of the internal compensation of individual ilmenite moments, partly due to frustrated spins.

Below T_N, for lamellae of equal area, the variability of the net lamellar moment corresponds to the ratio c_{CL} of coupled contact layers (Fig. 5, Table 1). It is thus controlled by the internal ilmenite compensation. Changes of the precise lattice parameters with temperature are of little influence for the models and therefore were not taken into account.

The details of lamellar shape depend on bulk chemistry and thermal history. The modelled values of c_{CL} in Table 1 cover the total range of experimentally determined ratios $M_{r,AV}$ /NRM_Z from 0.82 to 0.53. The experimental results represent averages from thousands of lamellae of widely different shapes and ratios, and are compared here to theoretical models of a single lamella with a single ratio.

The model ratios are indicative of average behaviour in the natural samples. Because the samples are metamorphosed clastic sedimentary rocks, there may have been compositional heterogeneities in the primary oxide grains. These were later modified by effects of regional metamorphism. The different specimens A–J come from four different rock cores with slightly different compositions and exsolution features (see McEnroe *et al.* 2016, tables 1 and 2). Composition differences could lead to different exsolution features, even though all the samples originate from the same outcrop and essentially had the same cooling history. Specimens A, C and G (Table 1) are from sample 22-6 and show high ratios 0.667, 0.760 and 0.721. B and H are from sample 22-2-1b and show low ratios 0.592 and 0.578. Specimens E and J come from 22-8a and also show low ratios 0.599 and 0.525. However, specimens D, F and I all come from sample 22-5 and show a wide range of ratios 0.576, 0.726 and 0.820. The proposed linkage of the experimental ratios to features of lamellar shape is a concrete and highly attractive conclusion, though it cannot at present be reliably tested beyond what has been presented here. An alternative measure of linkage involves the different behaviour of specimens with different magnetic orientations of crystals in populations where one set of NRM orientations dominates over the other. This results in asymmetric bimodal exchange bias that can be quantified by the ratio of the larger loop opening to the total of both loop openings (B_{pk}/B_{Tot}) listed in Table 1. One immediately notes that these two measures of linkage are in poor agreement with each other for three specimens I, C and F (marked
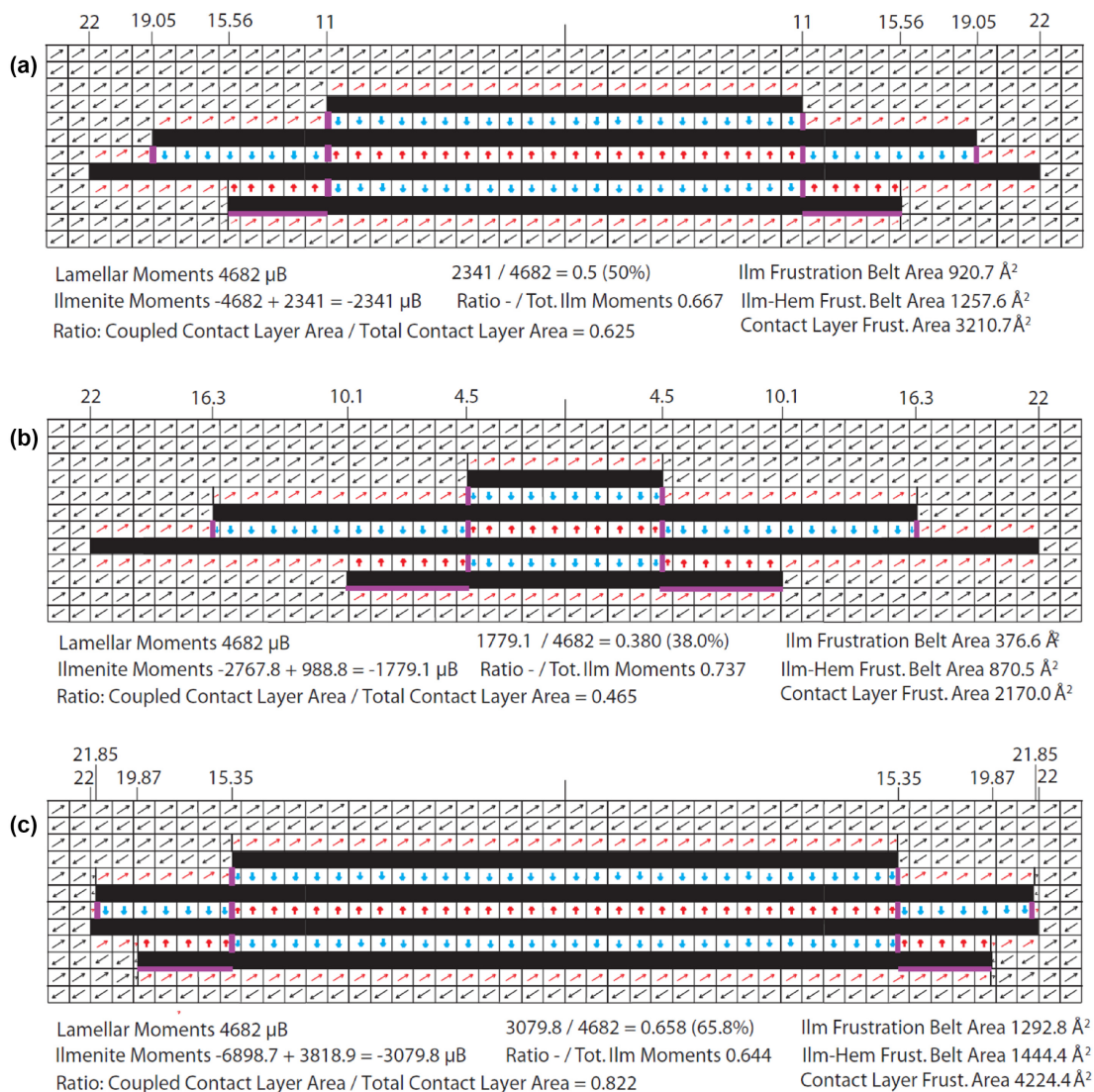
Figure 5. Full-diameter slices below $T_N = 57$ K across the final state of three lamellar growth models with (a) constant-volume, (b) decreasing-volume and (c) increasing-volume growth steps. In all cases the final step aspect ratio is 8.0. The fractions come from the use of circular disks, that do not correspond to an integer number of unit cell areas. Colour key: small red arrows, contact layer moments retaining approximate 300 K orientation; ilmenite Fe^{2+}-layer moments pointing down (heavy blue arrows) or up (heavy red arrows) normal to (001) as a result of antiferromagnetic coupling with lamellar moments; violet lines indicate surfaces of magnetic frustrations both parallel and normal to (001) as discussed in text.

by asterisks in Table 1), though the reason for this is unclear. Both sets of numbers are reasonably compatible with the c_{CL} ratios from the models (Table 1).

4 ACQUISITION OF LAMELLAR MAGNETISM AND CONSEQUENT LOW-*T* ILMENITE MAGNETIZATION

Understanding of this subject requires a background of knowledge of the hematite–ilmenite phase diagram and the most recent information on the magnetic properties of hematite and ilmenite, dealt with briefly above in discussion of Fig. 3.

4.1 Orientation and thermal effects

On the phase diagram (Robinson *et al.* 2004), the titanohematite compositions lie in a region where the Curie temperatures are in the range 900–820 K, substantially above 800–650 K, where small amounts of ilmenite exsolution would take place. Thus, under conditions where hematite is fully magnetized, an ilmenite component is contained in solid solution at a temperature where the free energy does not favour amalgamation of Ti-rich regions into discrete lamellae. The fact that exsolution does take place at lower temperature, means that diffusion rates of ions are sufficient to permit such amalgamation on the timescale of geological cooling. What then of the magnetic state within the titanohematite above the exsolution temperature? Before discussing the potential magnetic evolution of what one might term 'ionic soup', it is necessary to consider the magnetic structure of hematite itself. According to the studies of (Dzialoshinskii 1957) and continuing for the next 50 yr (Morrish 1994) it was understood that the oppositely pointing sublattice magnetizations in alternate Fe^{3+} cation layers are parallel to the (001) basal plane, but that a very slight misalignment ('canting') in that plane (a deviation of $\approx 0.1°$ from 180°) creates a ferromagnetic moment at 90° to the sublattice magnetizations. Further group

theoretical analysis (Harrison *et al.* 2010) shows that superposition of the magnetic structure on the rhombohedral cationic structure produces an overall monoclinic symmetry with magnetic space group *A*2/*a*. The spins are permitted to lie within the *a* glide plane at an arbitrary angle to the (001) basal plane. The spins are canted by a small angle out of the *a* glide plane, creating a net canted moment parallel to the diad in the (001) basal plane. In a neutron diffraction study of an exsolved titanohematite, (Harrison *et al.* 2010) found evidence for sublattice magnetizations tilted at 30° to (001) and thought this might relate to the exsolution interfaces. However, the same out-of-plane tilting, with angles somewhat less than 30°, was found in similar studies by (Brok *et al.* 2017) on several samples of unexsolved hematite. These symmetry features enter into consideration as to how titanohematite magnetizes above the ilmenite exsolution temperature, and how this relates to the lamellar magnetism created when stable lamellae form.

In order to understand hematite magnetization, one must recognize that any given titanohematite crystal is likely broken up into numerous cystallographic and magnetic domains. In any domain, one can expect the sublattice magnetizations to be oriented either $+30°$ or $-30°$ away from (001), as in Figs 3(a)–(c). Taking account of the symmetry change from rhombohedral to monoclinic imposed by magnetic ordering, there are six different domain characteristics that are possible within a single crystal, with spin-canted magnetic moments lying in six different directions exactly in the (001) plane. There will be a very slightly higher probability that those domains where the spin-canted moments are closest to the orientation of the magnetizing field will be predominant, but within the population, there will be some domains where the spin-canted moments will be antiparallel to the magnetizing field. The net magnetization of the single titanohematite crystal will be the collective sum of the diverse spin-canted magnetizations of all six types of magnetic domains, and will be substantially weaker than the magnetization of a single magnetic domain in ideal orientation with respect to the magnetizing field. Once the spin-canted domains are established, one must then consider what happens when exsolution is about to create ilmenite lamellae in each domain. The hexagonal plates in Fig. 3 are used to make tiny 'protolamellae' (Figs 6a and b) consisting within the plate of two Ti cations, flanked above and below by two contact layers, each containing one Fe^{3+} ion and one Fe^{2+} ion. Depending on placement in the hematite host, these would have either an upward (positive) or downward (negative) component of lamellar magnetism. These hexagonal units leave open the possibility of choosing one of three possible contact layer sublattice magnetization orientations within the six different potential domains. However, by having a magnetic field favour one of these three orientations, a simpler 'protolamella' can be described (Figs 6c and d) along a (1 1–2 0) plane consisting of 2 Ti cations, 2 Fe^{2+} cations and 2 Fe^{3+} ions flanked by hematite on both sides. Such 'protolamella' units, undoubtedly not fixed in one location until actual exsolution, nevertheless could play a role in reducing charge imbalance compared to a situation where Ti cations are isolated within hematite Fe^{3+} layers. Such units might also play a role in the magnetism of the host, and, unlike the surrounding purer hematite, these units could have local magnetic moments similar to lamellar moments, parallel to the tilted sublattice magnetizations, rather than the spin-canted ferromagnetic moments as in pure hematite that are normal to the sublattice magnetizations.

As stated above, the two contact layers of a lamella both have the same magnetic moment, and only the position of the Ti layer within the host, where alternate layers are oppositely magnetized,
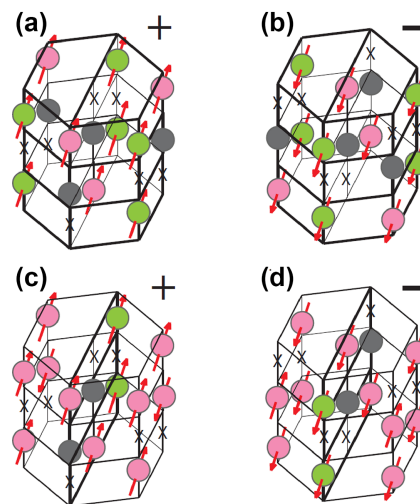

Figure 6. Protolamellae with opposite moments that would have to be placed differently in a magnetized hematite host. $+$ and $-$ indicate upward or downward vertical component of the lamellar moment. A and B show a protolamella of three layers with hexagonal unit-cell footprint, here showing one of three permitted potential orientations of lamellar moments and corresponding hematite moments. C and D show a smaller protolamella in a vertical plane (1 1–2 0) that could occur where the lamellar moment direction is already settled.

determines the magnetic moment direction of the lamella (Robinson *et al.* 2004). This concept is illustrated in Fig. 7 where two hexagonal 'protolamellae' with $+$ and $-$ moments are placed in a magnetized hematite host (layers 1+, 2–). When the contact layers are in odd-numbered layers (3+, 5+), the moments are $+$, when in even-numbered layers (2–, 4–) the moments are $-$. Fig. A1 in Appendix A illustrates the same placement concept, but using the simplified 'protolamellae' of Figs 6(C) and (D) occupying a vertical plane with hematite to both sides. If the sublattice directions are oriented at a low angle to the magnetizing field, there will be a slightly greater tendency for lamellae to form with Ti placed chemically to give lamellar moments as close as possible to the magnetizing field (the 'external force' hypothesis), thus $+$ 'protolamellae', as in Figs 7 and A1, will dominate. If the sublattice directions are oriented at a high angle to the magnetizing field, there will be little tendency for lamellae to form with Ti placed chemically so that lamellar magnetic moments will be in any particular orientation with respect to the magnetizing field (no external force effect), thus $+$ and $-$ 'protolamellae' will be equally abundant. Even in the most favourable orientations with respect to the field, thermodynamic considerations can cause many lamellae to settle in positions where their lamellar moments are contrary to the field direction. Even if only a small proportion of the lamellae adopt moments towards the field direction, a considerable moment can be achieved. We speculate here that this external force effect might occur also within unexsolved titanohematite hosts as a result of an external force effect on what we here call "protolamellae". If so, the local "protolamellae" moments, are much stronger than the local spin-canted moments, and these may cause the sublattice magnetizations of the titanohematite crystals to lie as close as possible to the magnetizing field, rather than normal to it, as would be the case if the weak spin-canted moments were dominant. All this emphasizes that hematite domain structure cannot be ignored in the acquisition of lamellar magnetism. In summary, the sublattice orientations remain dominated by the magnetocrystalline anisotropy, and these will be dictated by the overall domain structure
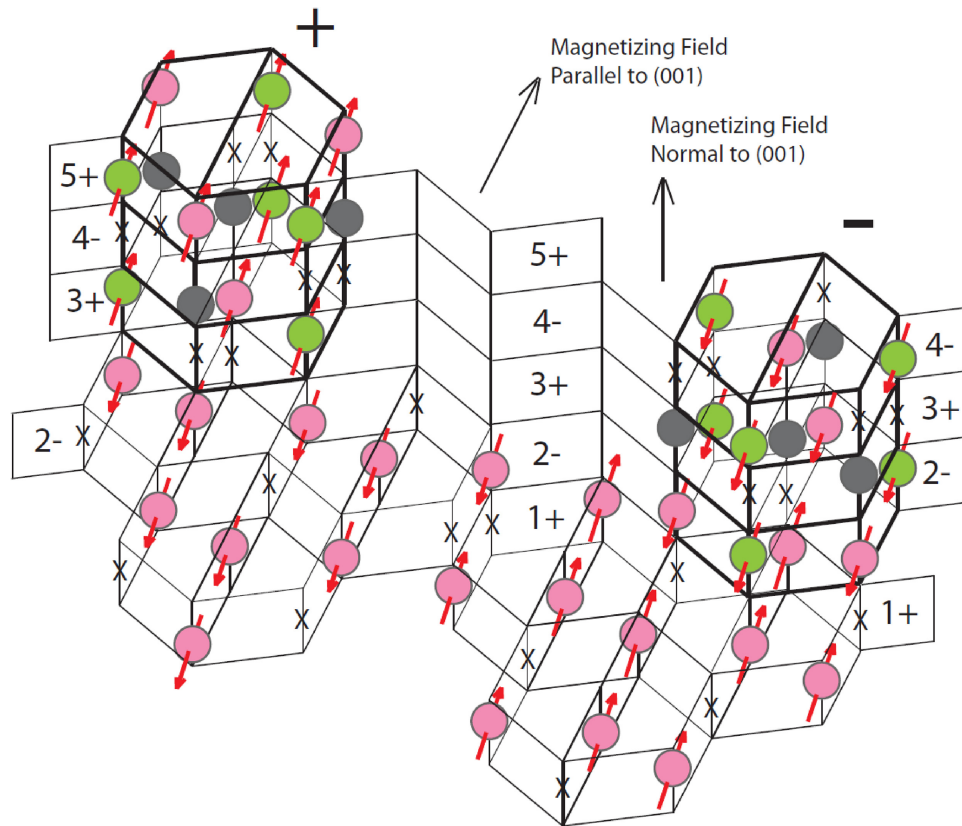
Figure 7. Two ilmenite protolamellae of three layers with hexagonal unit-cell footprint and showing one of three permitted potential orientations of lamellar moments and corresponding hematite moments. The protolamellae are in different vertical positions, hence have opposite lamellar moments in the same magnetized hematite host. Odd-numbered layers have a positive vertical component of the lamellar moment. Even-numbered layers have a negative vertical component of the lamellar moment. Protolamellae with components shown will be favoured during cooling in a magnetizing field parallel to (001). With a magnetizing field normal to (001), protolamellae with any one of three potential positive lamellar moment orientations will be chosen. Protolamellae with negative vertical components can occur due to thermal motion of cations. These will be most common when the magnetizing field is normal to (001).

of the parent grain. In each domain, the particular orientation of the sublattice moments will dictate the orientation of the lamellar moment. Those domains that have their sublattice moments favourably oriented with respect to the field will see a greater bias in the populations of + and − lamellae. Overall, the effect is that any pre-existing canted moment, caused by the imbalance of different-oriented domains, is overprinted by the lamellar moment. Thus, each crystal is a multidomain host, with six possible sublattice moment orientations (and six different canted moment directions) dictated by the magnetocrystalline anisotropy. There is a small imbalance between the populations of the six canted domains, which gives rise to the initial canted TRM of the host prior to exsolution. The net canted moment, averaged over all the domains, will be parallel to the field (in each individual domain, however, the canted moment is normal to the sublattice orientations). This pattern of domains forms the template for the later development of exsolution lamellae. In each domain, as lamellae form, there will be a bias of + versus − lamellae forming, creating a lamellar magnetism parallel to the sublattices. Further modelling avoids consideration of spin-canted moments, because the magnitude of lamellar magnetism is greater. The issue of domains is an important detail, but can be ignored in the modelling, where we deal with relative intensities of magnetization, rather than absolute values. One can also avoid the many complications that would be involved if the titanohematite hosts contain either true crystallographic twins or more complex magnetic twins, which are known to occur in some hematite (Tanner *et al.* 1988).

4.2 Comparison of modelled and experimental results

Both, 2-D and 3-D model and experimental results are plotted in Fig. 8. Here the horizontal axis, ranging from 0° to 180°, is the orientation of the NRM with respect to the positive field direction in the MPMS instrument. The vertical axis is plotted differently. When NRM angle is 0° to 90° so that the negative ilmenite moment dominates over the positive internal ilmenite moment, the plotted ratio is the *negative* internal ilmenite moment divided by total ilmenite moment. When NRM angle is 90° to 180° so that the positive internal ilmenite moment dominates over the negative internal ilmenite moment, the plotted ratio is the *positive* ilmenite moment divided by total ilmenite moment. Fig. 8 shows that the 3-D results for randomly distributed crystals have a similar form to the 2-D results, but the ratios with the NRM oriented close to 0° and 180° are substantially reduced. The cause of this is that the 3-D array contains a higher proportion of crystals with strong ilmenite remanences at high angles to the field than those with ilmenite remanences at low angles to the field. These make up a high proportion of the total ilmenite remanence, but are weakly expressed when the NRM is oriented at 0° and 180°. Of the 10 experimental results (blue circles), 5 are consistent with the model curves involving only randomly oriented crystals. Three of the remaining results are potentially capable of explanation if lattice-preferred orientation is taken into account, as discussed in Section 5. Two of the experimental results, B and E, have values seemingly beyond easy explanation using the present modelling approaches.
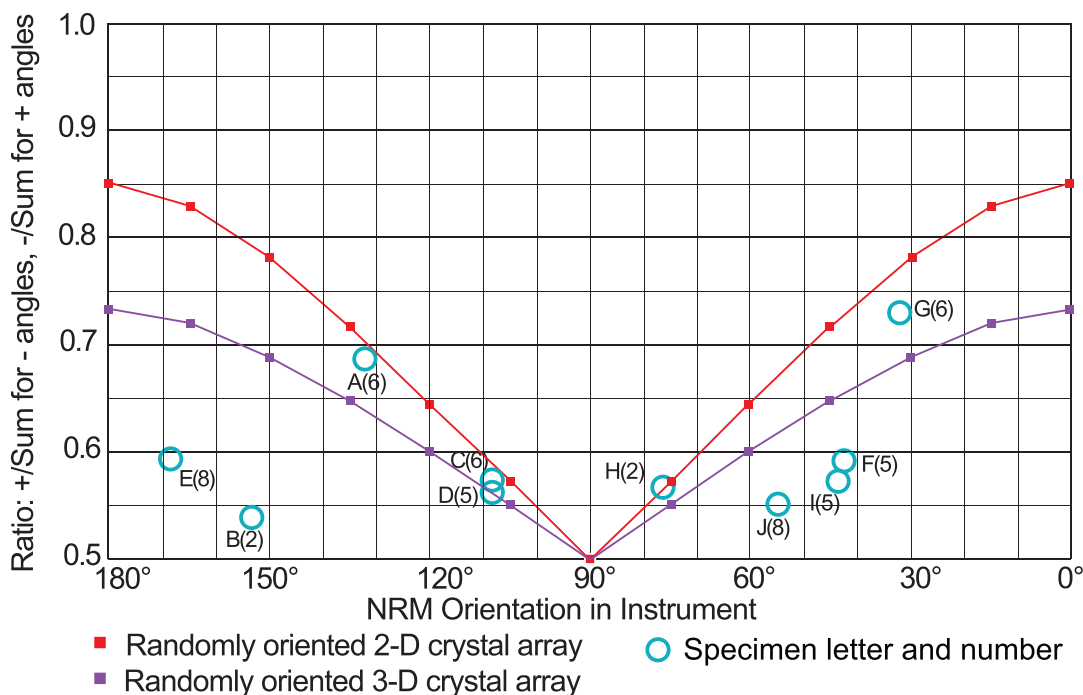
Figure 8. Plot of the ratio of the stronger low-*T* ilmenite moment to the total low-*T* ilmenite moment versus the orientation of the NRM in the MPMS, based on calculations for 2-D and 3-D lamella models given in Appendix B (and see figure A3). The corresponding values of B_{pk}/B_{Tot} (blue circles) are shown for the 10 sets of experimental results listed in Table 1. Note that negative peak values occur at positive orientations. Red squares indicate results from a 2-D model of randomly oriented crystals. Violet squares indicate results of a 3-D model of randomly oriented crystals.

5 LATTICE PREFERRED ORIENTATION (LPO) OF TITANOHEMATITE

A feature of the magnetism of titanohematite and hemo-ilmenite, covered earlier (Hargraves 1959; Robinson *et al.* 2006a, 2012), is the effect of LPO on magnetic intensity and NRM orientation. The Modum 22 samples were located where there is a strong steeply dipping planar deformation fabric. Two methods to study this phenomenon are (1) by measuring the anisotropy of magnetic susceptibility (AMS) and (2) by measuring populations of crystal orientation by electron backscatter diffraction (EBSD). Comparisons of these two approaches were provided by Robinson *et al.* (2012). Here we selected sample MOD22-6 for an EBSD study. The work was done on a polished 2.5-cm-diameter circular cut across an oriented diamond drill core. The core had an azimuth of 12° and a plunge of 68°. Thus, the circular cut was 22° from horizontal. Laboratory procedures were described by Robinson *et al.* (2006a), and Fabian *et al.* (2011). Results are illustrated in Fig. 9. The upper part of the figure shows three equal area diagrams with the orientations of three different crystallographic directions 001, 100 and 110 of 2969 points. The lower part of the figure shows the same results with contours at 0.5, 1, 2, 3 and 4 multiples of uniform density (mud) with a maximum at 4.77 mud. One might speculate that a substantial number of measuring points come from different parts of larger-than-average crystals with a common orientation. The two parts of Fig. 10 demonstrate conclusively that this is not the case. Fig. 10(a) is a backscatter electron image, where titanohematite shows as bright areas. Fig. 10(b) is an orientation contrast image in grey scale. This shows different orientation contrasts within the large areas of titanohematite, and all of these are smaller than the 100 μm step size used.

The plot of 001 in Fig. 11, that is the *c*-crystallographic axes or poles to (001), shows a very strong planar lattice-preferred

orientation of (001) with a very steep dip, and shows that this concentration lies along a side-to-side girdle. The girdle is likely to be the result of slight folding of a foliation of the (001) planes related to sub-horizontal fold axes found locally, and in the nearby region. One can look at the results for 100 and 110 for any evidence for a lattice-preferred orientation of a-crystallographic axes within the oriented (001) planes. If present, this could be pertinent during acquisition of magnetization. Both diagrams show a slight concentration of points in a quasi-horizontal direction normal to the (001) girdle. However, this concentration, slightly above 2 per cent, is most likely related to the same folding effect of (001) planes already discussed and not related to a significant LPO of a-axes in the plane of (001). Further attention here is only on (001). The upper part of Fig. 11 shows the contoured poles to (001) reoriented to the correct 12° (east of north) azimuth position but with the core axis still vertical. The lower part of Fig. 11 shows critical data from the top part in lower hemisphere projection tilted by 22° so that the core axis and other features are in original geographic orientation, including the 'fold axis' directly related to the *c*-axis girdle. In this corrected position, the statistical (001) of titanohematite strikes N 22°E and dips 74°E (mean pole at $D = 292°$, $I = 16°$). This is compared here with a reversed Proterozoic magnetic vector at $D = 276°$, $I = -67°$ (McEnroe *et al.* 2016), which when projected onto the lower hemisphere, is only 6° from the statistical (001) plane, indicating that this LPO could be significant in relation to the intensity of lamellar magnetism.

5.1 Summary of results of 2-D application of LPO

In order to model the range of possible effects of the relative orientations of the field and crystallographic axes, we smoothed the (001) orientation distribution obtained from EBSD along the girdle
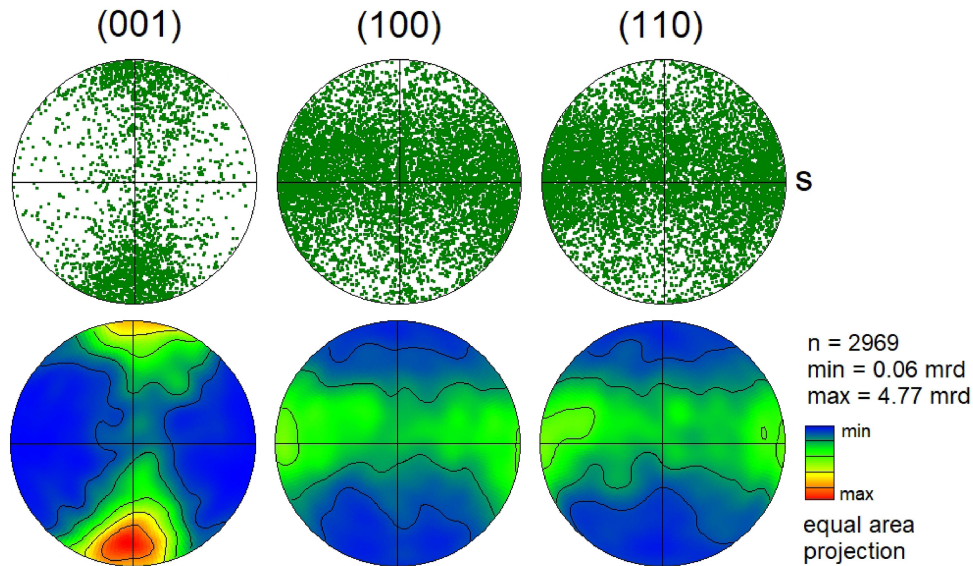
Figure 9. EBSD study of a single MOD-22-6 core in which 2969 titanohematite grain orientations were measured. Note the strong lattice-preferred orientation of (001) planes in left two images.
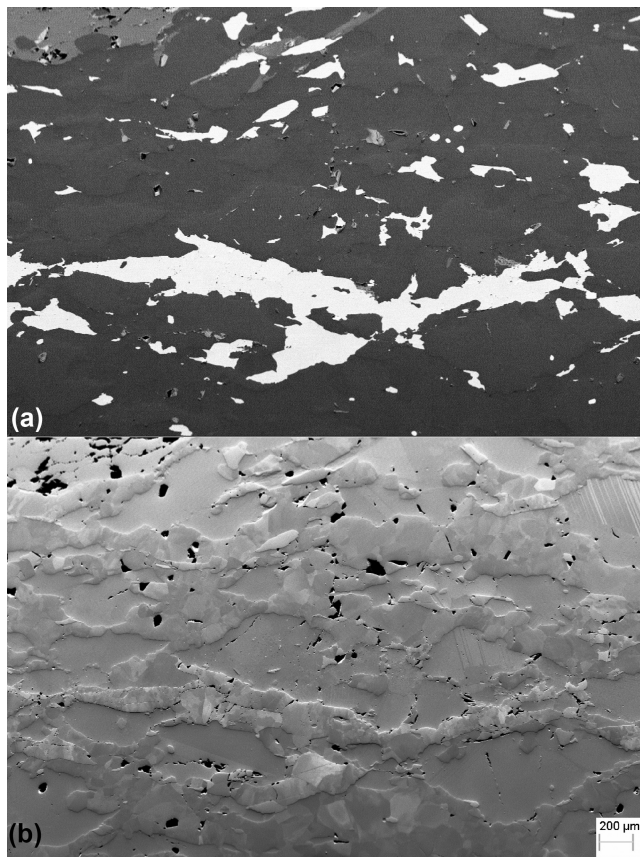

Figure 10. Sample MOD-22-6. (a) Backscatter electron image where titanohematite grains are bright areas and silicate grains are grey. Ilmenite lamellae in titanohematite are too small to be observed at this scale. (b) Orientation contrast image in grey-scale showing different orientation contrasts within the large areas of titanohematite, all smaller than the 100 μm step size used in the EBSD study. Note scale bar is 200 μm for both images.

(Fig 11), tabulated values for angles of 0°, 18°, 36°, 54°, 72° and 90° from the central high concentration, and normalized these by the lowest value to obtain a set of multipliers to be applied to intensities of the random-orientation model of Fig 8. These multipliers range from 1 to 4.75, and can be applied to different angles with respect to the field, to simulate various angular relationships between field and rock fabric.

The first magnetic test of the 2-D approach was made by placing the strongest multiplier, 4.75, at 180°, which is 90° from the magnetizing field. As expected, when rotated over 180° with respect to the MPMS, this gave a symmetrical set of results as shown by the violet points in Fig. 12 and decreased intercepts at 180° (−0) and 0° (+0) orientations compared to the red points of the randomly oriented array in Fig. 8. The envelope between those red points and the violet points includes the results from 5 out of the 10 natural specimens. The second magnetic test of the 2-D approach was made by placing the strongest multiplier, 4.75, on crystals at 90° that are normal to the natural magnetizing field. As expected, this also gave a symmetrical set of results as shown by the blue points in Fig. 12, but with increased intercepts at 180° (−0) and 0° (+0) orientations compared to the red points of the randomly oriented array in Fig. 8. This effect is the result of heavier weighting on crystals normal to the field and weaker weighting on crystals parallel to the field. The envelope between the red points in Fig. 8 and the blue points in Fig. 12 includes no results from the 10 natural specimens, and there is no indication that any of the natural samples have an LPO with such a relation to the magnetizing field. Additional tests were made by placing the strongest multiplier, 4.75, successively in the positions at 162°, 18°; 144°, 36°; 126°, 54°; and 108°, 72° (alternatively expressed as ±18°; ±36°; ±54° and ±72°) ; where + and − positions give similar results, but in mirror-image arrangement (Fig. 13). In all of these sets the values at 180° (−0) and 0° (+0) are identical and the actual values are in a consistent progression between the values for the symmetrical settings (Fig. 12), which are lowest when 4.75 is placed at 0° and highest when 4.75 is placed at 90°. All of the asymmetric results in Fig. 13 show 0.50 vertical ratios well away from 90°, varying from 81° down to 68°. The envelope of all the asymmetric results contains the same 5 results
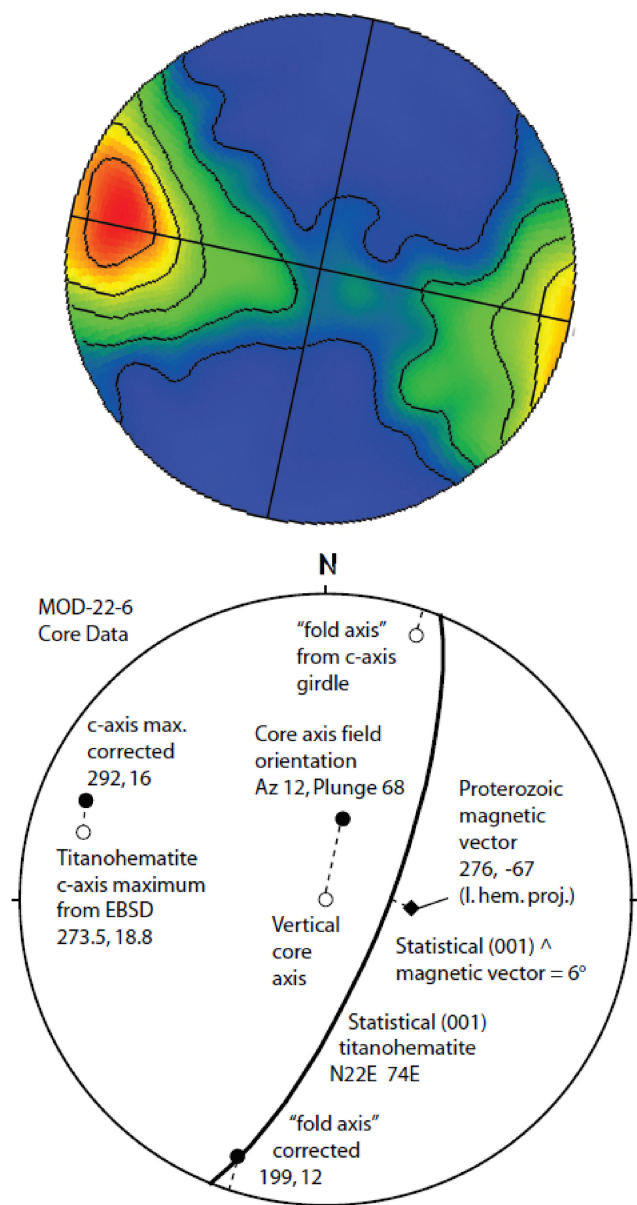
Figure 11. Top panel: contoured EBSD diagram re-oriented to core azimuth. Bottom panel: esults in lower hemisphere projection tilted 22° to true geographic orientation. The statistical titanohematite (001) foliation and the reversed Proterozoic paleomagnetic vector, projected to lower hemisphere, are separated by an angle of only 6°; highly favourable for obtaining a strong lamellar NRM.

from natural samples, but comes very close to including 3 more (J, I, F), leaving only E and B well away from any model results. It is encouraging to be reminded that the natural geometric and EBSD conditions illustrated in Fig. 11 come closest to the model conditions, where the strongest multiplier is placed either symmetrically at 0° or asymmetrically at 18°.

The net effect of Section 5 is an improvement in the agreement between the experimental and calculated values now collectively portrayed in Figs 12 and 13. The main points are that the distribution of crystal orientations has an impact on the magnetic behaviour, and that including the texture measured by EBSD into the models improves the agreement.

5.2 Summary of effects of LPO on NRM orientation and low-T hysteresis: 3-D analysis

To apply the chosen LPO, as in Fig. 11, to a 3-D analysis for randomly oriented crystals one can use the 3-D EBSD record of the oriented crystals, plotting the maximum horizontal at 180°, and the girdle vertical oriented E–W. By applying these weighting factors to random 3-D results produced with the magnetizing field set at 90° one obtains an array of weighted ilmenite moment intensities that is repositioned at 18° intervals. Then, for each of these positioning arrays, the relative positive and negative ilmenite intensities could be recorded as each positioning array was rotated from 180° to 0°. The ratios derived from the randomly oriented model are portrayed in Fig. 8.

6 RATIONALIZING MODELS WITH HYSTERESIS RESULTS – THE EFFECT OF DOMAIN WALLS

Here we explore how exsolution lamellae grow and the consequences this has on lamellar magnetism at high T between the Néel temperatures of hematite and ilmenite. We then examine the magnetization and magnetic anisotropy at low T below the Néel temperature of ilmenite. We consider how the effects of different populations of lamellae with respect to the magnetizing field may influence the intensity of the lamellar moment at high T and the ilmenite moments at low T. We then show how a changing orientation of the bulk NRM of a collection of lamellar crystals recorded at high T can affect the relative size and positions of hysteresis loop openings at low T by using 2-D and 3-D models of crystal collections. First, we assume random geometrical distributions of crystals, and then distributions of crystals with lattice-preferred orientations. For some of the latter we employed a real LPO on one the samples measured by EBSD involving 2969 crystal points. We compared these model results with numerical results obtained from the 10 samples. Now focus is placed on the various morphological features of the low-T hysteresis loops and their origin. The general questions to be answered here include the following:

(i) Why are the bimodal NRM loops, illustrated by peak shapes, so asymmetric, with long extensions on the high-field sides and steep slopes on the low-field sides?
(ii) Why is the exchange bias larger for the smaller of the two bimodal peaks than for the larger peak?
(iii) Why are the exchange bias values of the NRM loops so much larger than the values for field-cooled (FC) loops, acquired by cooling the specimens in a 7 T field from room-temperature to low T?

Fig. 14 shows the sets of NRM and FC hysteresis loops from Paper II for specimens D and G, with several quantitative features highlighted. For D the NRM vector was placed in a negative orientation, resulting in a larger positive-field loop opening and graphic peak (i.e. the location in a graph of the largest vertical dimension of a hysteresis loop opening). For G the NRM vector was placed positive, resulting in a larger negative loop opening and graphic peak. Also shown are the hysteresis shifts measured by two methods. The plain numbers and thin lines indicate the positions in T for the shifts based on the peak positions. The bold numbers and thick lines indicate the positions in T for the shifts based on the peak areas. For the NRM loops the shifts measured by peak area are consistently larger, in agreement with observations of peak asymmetry.
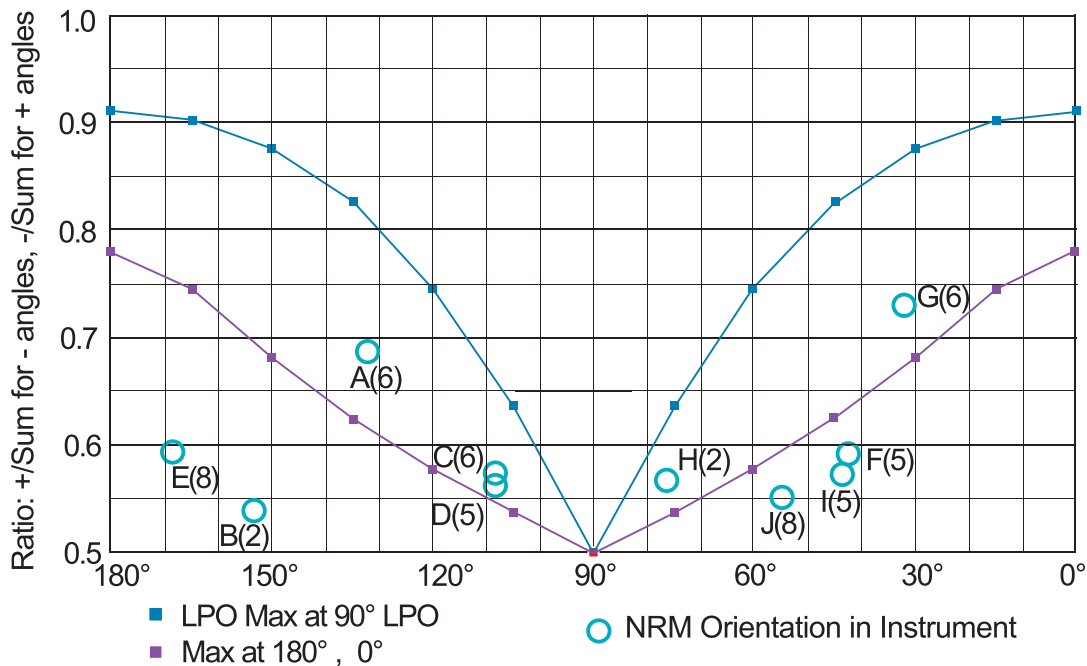
Figure 12. Test of symmetrically placed LPO multipliers in the 2-D model, placing the strongest, 4.75, in positions at 180°, 0° or 90°. In both sets, values with NRM at 180° and 0° are identical. Here the natural geometric and EBSD conditions illustrated earlier are closest to model conditions where the strongest multiplier is placed symmetrically at 180°, 0° and farthest to model conditions where the strongest multiplier is placed at 90°. Plotted is the ratio of the stronger low-*T* ilmenite moment to the total low-*T* ilmenite moment versus the orientation of the NRM with respect to the MPMS field direction. Equivalent values (blue circles) are shown for the ten sets of experimental results. Violet squares indicate results from a 2-D model where the maximum of the measured LPO is oriented at 90° to the MPMS axis. Blue squares indicate results of 2-D models where the maximum of the measured LPO is oriented at 180° and 0° to the MPMS axis.
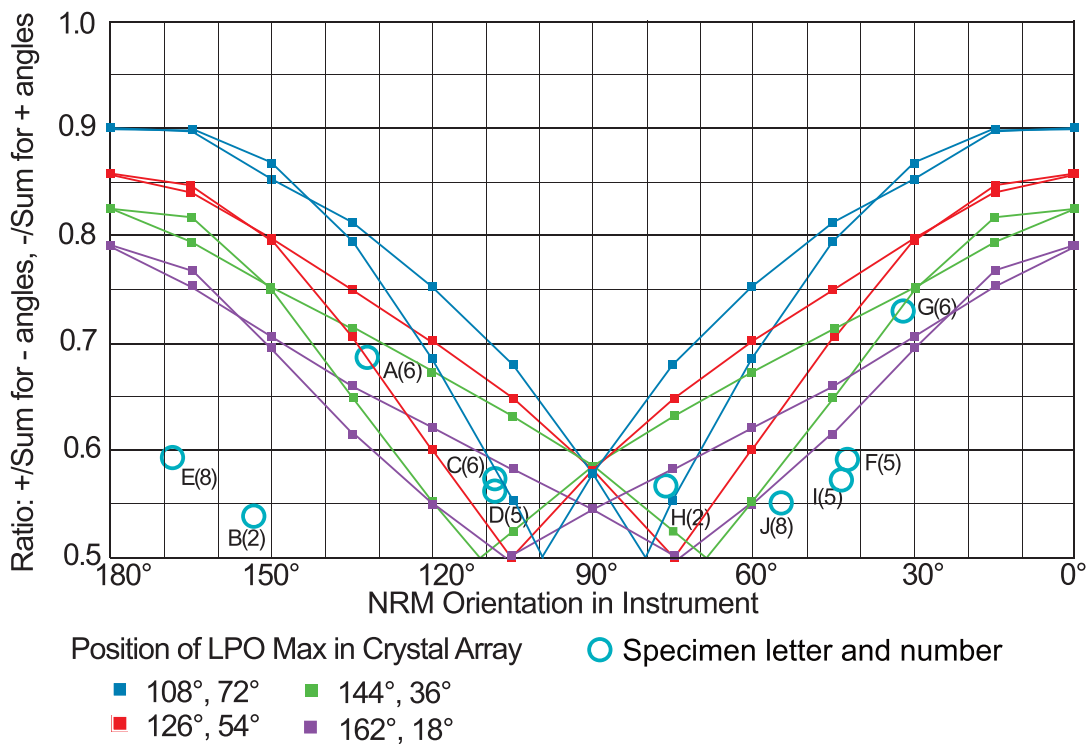

Figure 13. Test of asymmetrically placed LPO multipliers in the 2-D model as described in the text. Axes and measurement points are the same as in Fig. 12.
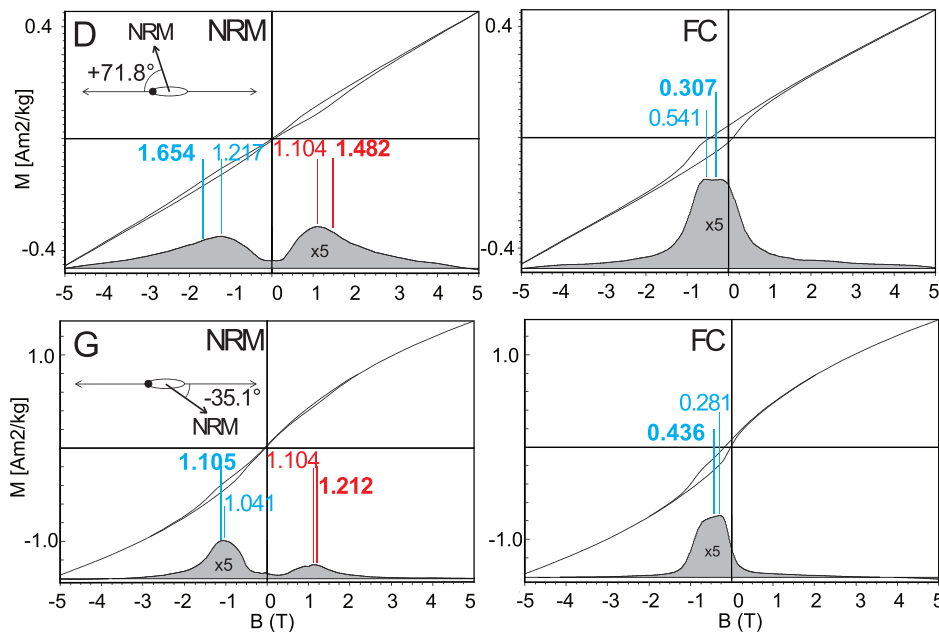
Figure 14. Low-*T* hysteresis loops of NRM and FC states for two characteristic samples D and G. Marks show hysteresis shifts, whereby thin numbers and thin lines indicate shifts measured by ΔM peak positions. Bold numbers and thicker lines indicate shifts measured by the median field of the peak area. The NRM of sample D was oriented negatively with respect to the measurement direction, giving rise to a bimodal loop with a predominant ΔM peak at positive fields. The NRM of sample G was oriented positively, giving rise to a bimodal loop with a predominant ΔM peak at negative fields.

A partial answer for the NRM loop asymmetry comes from consideration of the exchange coupling itself, as was briefly outlined in Paper II. It takes considerable field strength to bring the major component of the lamellar magnetism from the equilibrium state, working against exchange coupling of the ilmenite, into the exchange-biased state and to even stronger magnetizations beyond the peak. For the positive field this happens for crystals where positive ilmenite remanence predominates. For the negative field this happens for crystals where negative ilmenite remanence predominates. However, this effect is enforced during application of fields by the creation and movement of magnetic domain walls, where the initial NRM state in zero field has no domain walls due to rotated lamellar moments, even though the equilibrium population of lamellae contains a large fraction of lamellae with opposite magnetic moments.

6.1 Key role for domain walls in the hematite host — NRM loops

To explore the issue of domain walls, two different hypothetical crystals with (001) planes dipping 72° and 90° as indicated. have been selected, and here they are placed at the top of Fig. 15. These would have exsolved at high *T* in a field oriented vertically upward [inclined 18° to (001) in the crystal on the left, and parallel in the one on the right]. Some proportion of the newly formed lamellae will form in the stacking sequence such that their moments are nearly antiparallel to the ambient field, as in Fig. 6; these negatively magnetized lamellae are shown in blue in Fig. 15. To simulate conditions in the low temperature experiments, we rotate the two crystals counter-clockwise by 15°, so that they will be oriented appropriately with respect to the experimental applied field axis, here taken to be horizontal and in the plane of the figure. Then the ilmenite was magnetized on ordering at low *T* attaining ilmenite moments proportional to the cosine of the angle of the lamellar magnetism

to the original magnetizing field in nature, governing the fraction of negatively magnetized lamellae, as described in Section 4. Proportional ilmenite moments 0.866 and 0.669 are indicated. In addition, as a concept aid, each crystal is shown containing 30 ilmenite lamellae with different populations of originally positively magnetized lamellae (pink) and originally negatively magnetized lamellae (blue). One crystal with lamellar sublattice orientation closer to the magnetizing field has only two negatively magnetized lamellae. The other with a larger angle to the magnetizing field has 5 negatively magnetized lamellae. As mentioned above, the 2 selected crystals have both been rotated 15° counter-clockwise to magnetically useful orientations (−75° and +87°, as indicated in Fig. 15), to study the effects of applying strong fields along the MPMS axis, positive to the right and negative to the left. Magnetic walls in hematite are regions separating areas with one sublattice orientation from those with the opposite orientation, hence these are regions where the local sublattice orientations undergo a rotation of about 180°. Magnetic domain wall studies suggest such walls are likely several hundred nanometers thick. Thus, it is impossible to show the true extent of such walls in hypothetical crystals with only a handful of lamellae as in Fig. 15. The real situation during application of fields is that 'rafts' taking up parts of crystals with many lamellae, can break up into domains in which either positively or negatively magnetized lamellae predominate, but each retaining lamellae of the opposite magnetic polarity, according to the way they fit into the stacking sequence. When walls around individual crystals are shown, as in Fig. 15, this must be considered as schematic only and for the magnetization in the strongest fields, not for transitional conditions, though it does show more or less the general effect of magnetic walls.

The top part of Fig. 15 shows the two crystals after cooling to 5 K in the absence of a field, with the two populations of lamellae. On the right, 28 out of 30 lamellae have an original positive remanence, and only two have original negative remanence, but in the
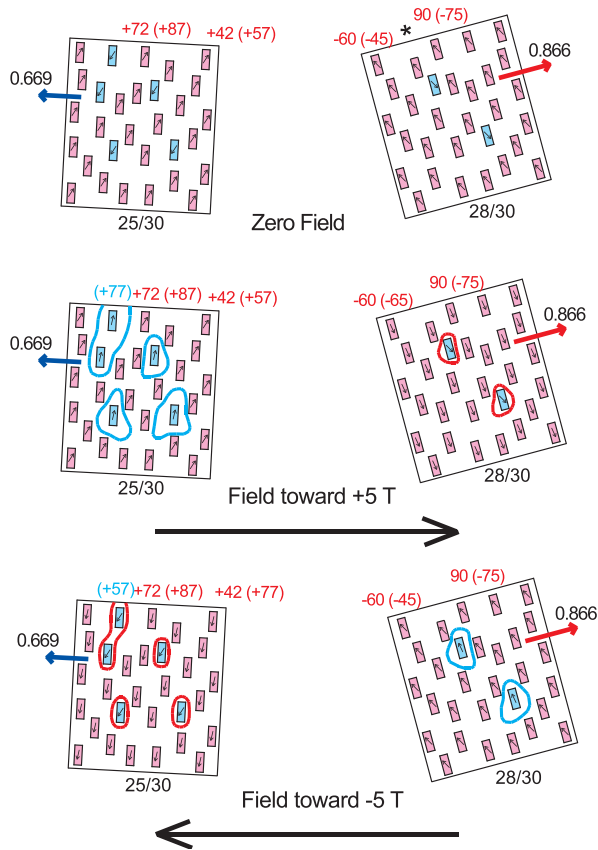
Figure 15. Representation of two crystals with ilmenite lamellae. These acquired a lamellar magnetism in a field directed vertically upward (90). The two theoretical crystals were then cooled in zero field to 5 K, thus acquiring ilmenite magnetic moments, and then rotated counter-clockwise 15° to the present position (top 2 crystals) in the figure. Application of a +5 T field (central 2 crystals) causes re-orientation of all originally negatively oriented lamellar moments (pink to right, blue to left) into a positive exchanged-biased state, in process creating new domain walls moving away from the shifted pink lamellae on the right (red domain wall) and the shifted blue lamellae on the left (blue domain wall). Application of a −5 T field (bottom 2 crystals) causes re-orientation of all originally positively oriented lamellar moments (blue to right, pink to left) into a negative exchanged-biased state, in process creating new domain walls moving away from the shifted blue lamellae on the right (blue domain wall) and the shifted pink lamellae on the left (red domain wall).

present position, the original positive lamellar remanences project as negative on the MPMS axis. The resulting cumulative ilmenite remanence is positive (with respect to the MPMS coordinates), indicated by the large red arrow. If a low-T hysteresis loop at $T < T_N$ were run on this crystal alone it would show unimodal positive exchange bias. On the left, 25 out of 30 lamellae have an original positive remanence, and 5 have an original negative remanence. In the present orientation, the original positive lamellar remanences would still project as positive on the MPMS axis. The resulting cumulative ilmenite remanence is negative, as indicated by the large blue arrow. If a low-T hysteresis loop were run on this crystal alone it would show negative exchange bias. The first hypothetical magnetic experiment involves high-field hysteresis after cooling in zero field, so the lamellar moments still retain their NRM configuration; we begin with application of fields up to +5 T. For the crystal on the right, the minority blue lamellae already have a positive moment with respect to the applied field and will change relatively little.

The majority pink lamellae will reorient towards the exchange-biased state, which we estimate will involve rotation of both the lamellar moments and eventually all the surrounding hematite moments by about 150°. A full rotation of 180° would bring it too close to the magnetically unfavourable position of being parallel to the ilmenite moments of the lamellae (Harrison *et al.* 2007). When this rotation begins, magnetic domains walls will form, separating the dominant pink lamellae and hematite host from the minor blue lamellae, and as the rotation proceeds the domain walls will converge towards the minority blue lamellae and also provide considerable resistance to the change of orientation. Thus, here is another explanation of the asymmetry of the positive peak, particularly well shown in Fig. 14, specimen D.

For the crystal on the left, the majority pink lamellae already have a positive moment and will change relatively little. The minority blue lamellae will be reoriented drastically towards the positive exchange-biased state, involving rotation of both the lamellar moments and all the surrounding hematite moments by about 160°. When rotation begins, magnetic domains walls will form between the dominant, relatively fixed, pink lamellar moments and the lesser rotating blue lamellar and surrounding hematite moments. As the rotation proceeds, the domain walls will move slightly away from the minority blue lamellae and provide some resistance to the change of orientation.

The second hypothetical magnetic experiment continues the low-T high-field hysteresis loop, by sweeping the field down to −5 T. For the crystal on the right the majority pink lamellae, already in the zero-field-cooled state, have a negative moment and will change relatively little. The minority blue lamellae will reorient about 160° towards the exchange-biased state. When this rotation begins, magnetic domain walls will form between the dominant pink lamellae and the minor blue lamellae, and as the rotation proceeds the domain walls will diverge towards the majority pink lamellae and also provide considerable resistance to the change of orientation.

For the crystal on the left, the minority blue lamellae already have a negative moment and will change relatively little. The majority pink lamellae will be reoriented drastically towards the negative exchange-biased state, involving rotation of both the lamellar moments and all the surrounding hematite moments by about 160°. As soon as this rotation begins, magnetic domain walls will form between the minority, relatively fixed, blue lamellar moments and the majority rotating pink lamellar and surrounding hematite moments. As the rotation proceeds the domain walls will move towards the minority blue lamellae and provide major resistance to the change of orientation. This helps to explain the asymmetry of the negative peak, as in Fig. 14, specimen D.

More important is to note that the amount of domain wall for the left crystal in a negative field, is more than the amount of domain wall for the right crystal in a positive field, thus creating greater resistance to change in a negative than in a positive field. This domain-wall feature provides a clear explanation for why the hysteresis shifts are almost consistently larger for the lesser peak than for the greater peak in these bimodal NRM loops. Potentially, in this case, the larger domain wall areas have an important hysteresis effect.

6.2 Key role for domain walls in the hematite host − FC loops

Now to the matter of the FC loops as compared to the NRM loops. Such a progression is illustrated in Fig. 16, beginning at the top,
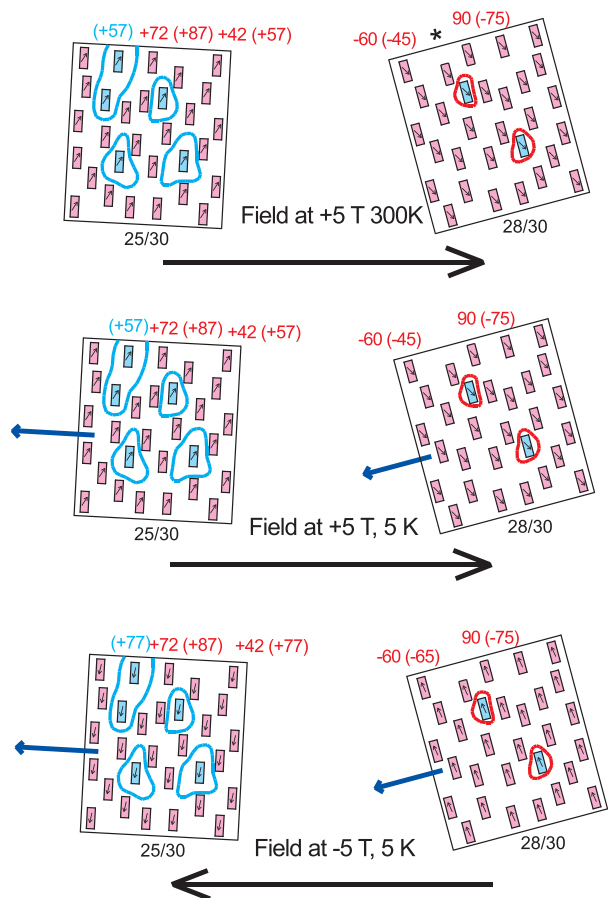
Figure 16. The same two crystals with ilmenite lamellae as in Fig. 15, now at 300 K following the low-*T* NRM hysteresis experiment and in a +5 T field (top 2 crystals). All originally negative lamellar moments (blue lamellae on right, pink lamellae on left), have been re-oriented to positive, creating domain walls that moved away from shifted lamellae (red on right, blue on left). Next (central 2 crystals) we see the result of cooling to 5 K in the +5 T field causing all lamellae to acquire a negative ilmenite moment normal to (001), due to antiferromagnetic coupling with the all positive lamellar moments. Domain walls remain as at 300 K. With the bottom 2 crystals, we see the result at 5 K of changing the field from +5 T to –5 T. The negative ilmenite moments remain unchanged, whereas all of the lamellar moments are changed to the exchanged-biased state. The domain walls originally created at 300 K must stay in approximately the same positions, but may change by moving slightly towards or away from different populations, and seem to have a muted effect on details of exchange bias. The net effect is a consistent unimodal negatively shifted exchange bias much smaller in magnitude than the shifts in the bimodal NRM loops, where domain walls are created and moved during the hysteresis.

where the same two crystals in Fig. 15 are shown at 300 K in a field of +5 T. Because of the different placement of positively and negatively magnetized lamellae, application of the field to +5 T at 300 K will create magnetic domain walls, where no such walls were present, at least theoretically, in the NRM state. Here there is no ilmenite magnetization, hence no exchange coupling, and all the lamellar moments are free to move as close to the positive MPMS field as possible. Here we do not speculate on how extreme this could be, but only show the lamellar moments 30° from the respective (001) planes. This is all that is required, so that when cooling in the same field to 5 K, all the resulting ilmenite moments will be negatively oriented with respect to the MPMS coordinate system, as shown in the middle set of crystals in a +5 T field at

5 K. Once the domain walls are created, and the lamellar moments are exchange-coupled to ilmenite moments at low *T*, the walls must remain present throughout the low-*T* hysteresis loop.

A remarkable feature shown by the FC experiments described in Paper II is that the negative internal ilmenite magnetization is acquired in a positive field of 5 T, and appears to persist from that condition through all other conditions during hysteresis. In fields decreased from +5 T to –5 T at 5 K, most of the lamellar moments have changed from the equilibrium state to the exchange-biased state.

It appears that the very much lower exchange bias of the unimodal FC loops compared to the bimodal NRM loops relates to the fact that the process of hysteresis of NRM loops involves the creation and movement of domain walls in the hematite host, where such walls are lacking in the field-free cooled condition. By contrast, the application of a strong field at 300 K before field-cooling to 5 K ensures that domain walls are present throughout the hysteresis experiment, not created during the experiment, and also that domain wall movement is less directed because the lamellar moments in all domains are in continual change during all parts of the loops. In examination of the FC loops, all showing negative shifts with an average ΔM peak position of 0.36 T (Table 6 in Paper II), we have found no obvious explanation for why some show a larger shift based on peak position, and others show a larger shift based on median peak area. We had a vague suspicion that the FC hysteresis shifts might be different in samples originally placed negatively in the MPMS than in samples placed positively, but no amount of averaging of the FC data from Table 6 in Paper II shows any difference.

7 CONCLUSIONS

We have shown that the shapes of the edges of ilmenite lamellae against their hematite hosts can control the degree of low-*T* AF coupling between ilmenite, and the lamellar magnetic moments. Some of the degrees of coupling agree with measurements made at low *T* on the natural samples. The high-*T* growth of ilmenite lamellae and their magnetic moments, as well as the low-*T* acquisition of magnetization of the ilmenite inside the lamellae, are controlled by the magnetic behaviour of Fe ions adjacent to Ti-rich sites within the overall hematite host and its ilmenite lamellae. This behaviour has been modelled for hematite hosts containing ilmenite randomly oriented with respect to the magnetizing field, and also for hematite hosts containing ilmenite lamellae with lattice-preferred orientation, as determined by electron backscatter imaging on a typical core sample. Such an LPO strongly influences the intensity of remanent magnetization and consequent low-*T* internal ilmenite magnetic intensity, when oriented towards the magnetizing field. For samples showing bimodal low-*T* ilmenite remanence, we provide a tentative explanation for why populations of ilmenite lamellae in a host showing stronger ilmenite remanence (A) show a smaller exchange-bias shift, than for populations of lamellae in a host showing weaker ilmenite remanence (B) that show a larger exchange-bias shift. We suggest that this effect may be due to the larger area of domain walls in (B) than in (A).

ACKNOWLEDGEMENTS

DATA AVAILABILITY

No new data were generated or analysed in support of this research.

REFERENCES

Brok, E., Frandsen, C., Lefmann, K., McEnroe, S., Robinson, P., Burton, B.P., Hansen, T.C. & Harrison, R., 2017. Spin orientation in solid solution hematite-ilmenite, *Am. Mineral.,* **102**(6), 1234–1243.

Dzialoshinskii, I.E., 1957. Thermodynamic theory of "weak" ferromagnetism in antiferromagnetic substances, *Soviet. Phys. JETP,* **5,** 1259–1272.

Fabian, K., McEnroe, S.A., Robinson, P. & Shcherbakov, V.P., 2008. Exchange bias identifies lamellar magnetism as the origin of the natural remanent magnetization in titanohematite with ilmenite exsolution from Modum, Norway, *Earth planet. Sci. Lett.,* **268**(3–4), 339–353.

Fabian, K., Miyajima, N., Robinson, P., McEnroe, S.A., Ballaran, T.B. & Burton, B.P., 2011. Chemical and magnetic properties of rapidly cooled metastable ferri-ilmenite solid solutions: implications for magnetic self-reversal and exchange bias-I. Fe-Ti order transition in quenched synthetic ilmenite 61, *Geophys. J. Int.,* **186**(3), 997–1014.

Hargraves, R., 1959. Magnetic anisotropy and remanent magnetization in hemo-ilmenite from ore deposits of Allard Lake, Quebec, *J. geophys. Res.,* **64,** 1565–1573.

Harrison, R.J., McEnroe, S.A., Robinson, P., Carter-Stiglitz, B., Palin, E.J. & Kasama, T., 2007. Low-temperature exchange coupling between Fe$_2$O$_3$ and FeTiO$_3$: Insight into the mechanism of giant exchange bias in a natural nanoscale intergrowth, *Phys. Rev. B,* **76**(17), doi:10.1103/PhysRevB.76.174436.

Harrison, R.J., McEnroe, S.A., Robinson, P. & Howard, C.J., 2010. Spin orientation in a natural ti-bearing hematite: evidence for an out-of-plane component, *Am. Mineral.,* **95**(7), 974–979.

Kato, H., Yamada, M., Yamauchi, H., Hiroyoshi, H., Takei, H. & Watanabe, H., 1982. Metamagnetic phase transitions in FeTiO$_3$, *J. Phys. Soc. Jpn.,* **51**(6), 1769–1777.

McEnroe, S.A., Carter-Stieglitz, B., Harrison, R.J., Robinson, P., Fabian, K. & McCammon, C., 2007. Magnetic exchange bias of more than 1 Tesla in a natural mineral intergrowth, *Nat. Nanomat.,* **2,** 631–634.

McEnroe, S.A., Robinson, P., Miyajima, N., Fabian, K., Dyar, D. & Sklute, E., 2016. Lamellar magnetism and exchange bias in billion-year-old titanohematite with nanoscale ilmenite exsolution lamellae: I. mineral and magnetic characterization, *Geophys. J. Int.,* **206**(1), 470–486.

Morrish, A.H., 1994. *Canted Antiferromagnetism: Hematite,* World Scientific.

Pentcheva, R. & Nabi, H.S., 2008. Interface magnetism in Fe$_2$O$_3$/FeTiO$_3$ heterostructures, *Phy. Rev. B,* **77**(17), doi:10.1103/PhysRevB.77.172405.

Robinson, P., Harrison, R.J., McEnroe, S.A. & Hargraves, R.B., 2002. Lamellar magnetism in the haematite–ilmenite series as an explanation for strong remanent magnetization, *Nature,* **418**(6897), 517–520.

Robinson, P., Harrison, R.J., McEnroe, S.A. & Hargraves, R.B., 2004. Nature and origin of lamellar magnetism in the hematite-ilmenite series, *Am. Mineral.,* **89**(5–6), 725–747.

Robinson, P., Harrison, R.J. & McEnroe, S.A., 2006a. Fe^{2+}/Fe^{3+} charge ordering in contact layers of lamellar magnetism: Bond valence arguments, *Am. Mineral.,* **91**, 67–72.

Robinson, P., Heidelbach, F., Hirt, A.M., McEnroe, S.A. & Brown, L.L., 2006b. Crystallographic-magnetic correlations in single-crystal haemo-ilmenite: new evidence for lamellar magnetism, *Geophys. J. Int.,* **165**(1), 17–31.

Robinson, P., Harrison, R.J., Miyajima, N., McEnroe, S.A. & Fabian, K., 2012. Chemical and magnetic properties of rapidly cooled metastable ferri-ilmenite solid solutions: implications for magnetic self-reversal and exchange bias, II. Chemical changes during quench and annealing, *Geophys. J. Int.,* **188**, 447–472.

Robinson, P., McEnroe, S.A. & Jackson, M., 2016. Lamellar magnetism and exchange bias in billion-year-old metamorphic titanohematite with nanoscale ilmenite exsolution lamellae II: exchange-bias at 5 K after field-free cooling of NRM and after cooling in a +5 T field, *Geophys. J. Int.,* **208**(2), 895–917.

Sharma, M., Murugavel, S., Shukla, D.K. & De Groot, F. M.F., 2018. Reversal in the lattice contraction of α-Fe$_2$O$_3$ nanoparticles, *J. Phys. Chem. C,* **122**(17)), 9292–9301.

Shcherbakov, V.P., Fabian, K. & McEnroe, S.A., 2009. Mechanism of exchange bias for isolated nanoparticles embedded in an antiferromagnetic matrix, *Phys. Rev. E,* **80**, 174419.

Tanner, B., Clark, G. & Safa, M., 1988. Domain structures in haematite, *Philos. Mag. B,* **57,** 361–377.

APPENDIX A: 2-D GRAPHICAL MODEL OF NRM-INDUCED EXCHANGE BIAS

Fig. A2 sketches that acquisition of lamellar moments potentially occurs in six different orientations of hexagonal titanohematite plates. Each part of the figure shows two views of a titanohematite crystal. The left-hand view looks directly at the (001) plane with three potential sublattice orientations on the front side at 30° to the a crystallographic axes and another three invisible on the back side. The dashed arrows show the limits of sublattice magnetizations with respect to the magnetizing field with in-plane rotation of the crystal 60° in each direction. Each right-hand view shows a side view of the plate with the *c*-axes at different angles to the natural magnetizing field, 0°, 36°, 54° and 90°. In a real exsolving crystal, a thermodynamic equilibrium with a preferred positive field alignment occurs. For positive alignment, nature has the option to choose any one of the three positive sublattice magnetization directions (red arrows), though negative magnetization of some lamellae along the same direction would be possible as a result of thermodynamic probability (blue arrows). The dashed arrows in Fig. A2 show the limits produced by up to 60° of in-plane rotation of the crystals. Such rotations conceptually describe cones making 60° angles with the crystal *c*-axes (Fig. A4). In a crystal with the *c*-axis at 0°, all possible sublattice orientations lie at 60° to the magnetizing field and the field can have no preference effect on the direction of sublattice magnetization, but, once selected, the field can influence the intensity of the lamellar moment. In a crystal with the *c*-axis at 36°, one of the possible sublattice orientations is 24° to the magnetizing field is preferred and could occur together with a proportion of negative equivalents. In-plane rotation of the crystal up to 60° would bring the sublattice magnetization out to 49° from the magnetizing field with resultant likely weakening of the lamellar moment. In a crystal with the *c*-axis at 54°, one of the possible sublattice orientations at barely 6° to the magnetizing field is strongly preferred but still could occur together with a proportion of negative equivalents. In-plane rotation of this crystal up to 60° would bring the sublattice magnetization out to 50° from the magnetizing field with resultant weakening of the lamellar moment. In a crystal with the *c*-axis at 90°, one of the possible sublattice orientations now 30° to the magnetizing field is less strongly preferred and could occur together with a proportion
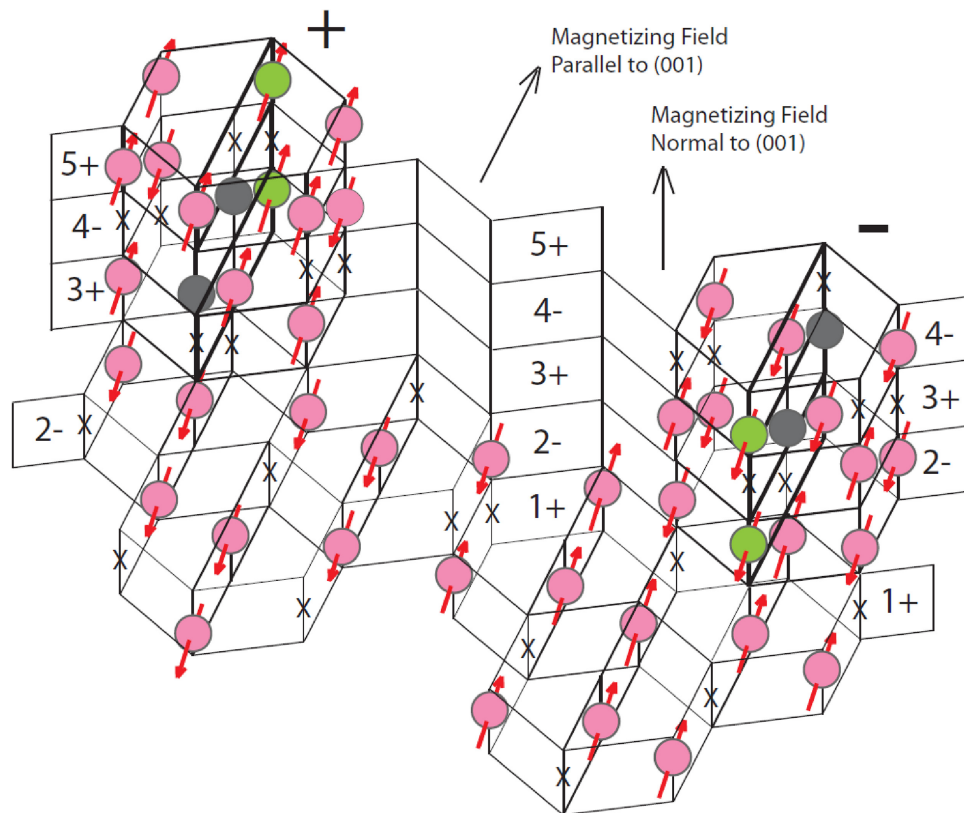
Figure A1. Two ilmenite protolamellae of minimal size with different vertical positions, hence opposite lamellar moments in the same magnetized hematite host. All ions in the protolamellae lie along the $(11-20)$ crystallographic plane. Odd-numbered layers have a positive vertical component of the lamellar moment. Even-numbered layers have a negative vertical component of the lamellar moment. Protolamellae with positive components in the orientation shown will be favoured during cooling in a magnetizing field parallel to (001). Protolamellae with negative vertical components may occur due to thermal motion of cations, and will be more common when the magnetizing field is at a high angle to (001).

of negative equivalents. In-plane rotation of this crystal up to 60° would bring the sublattice magnetization out to 64° from the magnetizing field with weakening of the lamellar moment. It is worth noting that the 'in-plane rotation' effect on the lamellar moment is strongest with the sublattice magnetization oriented parallel to the magnetizing field, and there is no effect when (001) is normal to the field.

APPENDIX B: THREE-DIMENSIONAL MODEL OF NRM-INDUCED EXCHANGE BIAS

The here described analytical calculations use several model assumptions for NRM acquisition within a hematite host containing a large population of nanoscale ilmenite lamellae. It is assumed that prior to lamella formation, the hematite host cools below its Néel-temperature of $T_N \approx 700\,°\mathrm{C}$ and becomes antiferromagnetic. It is further assumed that at these temperatures the Ti atoms still diffuse rapidly and behave like a magnetic gas or fluid inside the hematite crystal, because each Ti atom is associated with a defect moment of the hematite host. On cooling the Ti atoms arrange in energetically favourable states, leading to the formation of ilmenite lamellae below about $T_{exs} \approx 500\,°\mathrm{C}$.

For each crystal the external (e.g. geomagnetic) field at $T_{exs} < T < T_N$ interacts with the magnetic parameters of the host and the Ti-moments and influences the basal plane easy axis, the tilt direction of the hematite magnetization out of the basal plane, which involves

symmetry breaking with respect to the basal plane, and the field strength determines the Boltzmann statistics of the free Ti-related defect moments.

Below the exsolution temperature, changing the position of a lamella along the c-axis by one atomic layer within the antiferromagnetic hematite lattice, reverses its lamellar moment along c. The component of the lamellar moment within the basal plane is determined by the host and can assume any one of the three energetically equivalent easy directions. The experimental data show that the magnetic energy due to the geomagnetic field is large enough, to create a notable preference of field aligned lamellae over misaligned lamellae.

For the calculation of the average NRM, the coordinate system is chosen such that the NRM-field direction points in the z-direction of the coordinate system, and that the measurement direction **d** in the MPMS assumes an angle μ in the $x-z$-plane:

$$\mathbf{d} = (\cos\mu, 0, \sin\mu).$$

Using the polar angles θ, ϕ to describe the unit vectors

$$\mathbf{e}(\theta, \phi) = \begin{pmatrix} \sin\theta\cos\phi \\ \sin\theta\sin\phi \\ \cos\theta \end{pmatrix},$$

the probability to find a hematite c-axis orientation at the polar angles (θ, ϕ) is denoted by $p(\theta, \phi)$. To describe a tilt of the lamellar moment away from the c-axis, antipodal axis directions are chosen to correspond to different directions of the lamellar moment tilt
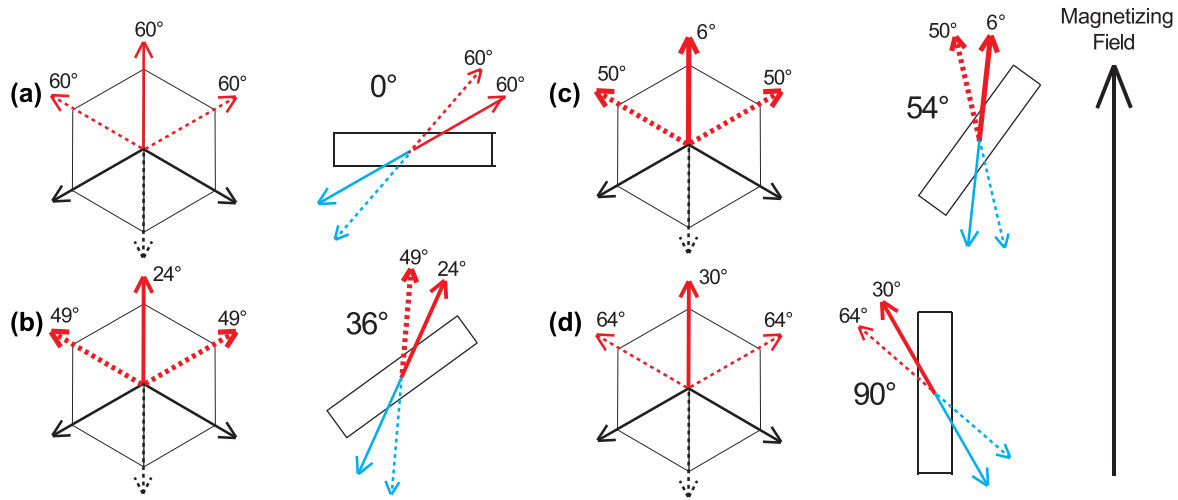
Figure A2. Relationships between hematite sublattice magnetizations 30° from crystallographic *a* axes and the natural magnetizing field for crystals with different orientations of (001). Arrows in the left images indicate three potential sublattice orientations relative to a hexagonal crystal. Dashed arrows indicate *a*-axes repositioned by 60° either way. Right images show (001) planes at various angles to the magnetizing field, with one set of sublattice directions. (a) Crystal (001) oriented at 0°, which is 90° from the natural magnetizing field. In this position the magnetizing field provides no preference in selection of sublattice magnetization, in all cases lying exactly 60° from the field. Once selected, thermodynamic phenomena could allow either positive (red arrows) or negative (blue arrows) moments of lamellae along that direction. This thermal effect is possible for other orientations. (b) Crystal (001) oriented at 36°, which is 54° from magnetizing field. In this position the natural magnetizing field would provide a strong preference for the sublattice magnetization to lie along the heavy arrow. Here the smallest angle of a sublattice magnetization to the natural magnetizing field is 24° (heavy arrow) and largest is 49° (dashed arrow). (c) Crystal (001) oriented at 54°, which is 36° from the magnetizing field. Here the natural magnetizing field provides the strongest preference for the sublattice magnetization to lie along the very heavy arrow. The smallest angle of a sublattice magnetization to the magnetizing field is 6° (heavy arrow) and largest is 50° (dashed arrow) with a difference of 44°. Of the four examples, this orientation is the one where the influence of the natural magnetizing field is strongest, and the effect of thermodynamic phenomena weakest, thus allowing the smallest proportion of lamellae with negative lamellar moments. (d) Crystal (001) oriented at 90°, parallel to the natural magnetizing field. In this position the magnetizing field would provide a strong, but not strongest, preference for the sublattice magnetization to lie along the heavy arrow. Here the smallest angle of the sublattice magnetization to magnetizing field is 30° (heavy arrow) and largest is 64° (dashed arrow) with a difference of 34°. Crystals oriented so that there are larger angles between the sublattice magnetization and the natural magnetizing field will obtain weaker lamellar magnetism, likely expressed by a higher proportion of lamellae with negative lamellar moments, resulting in weaker ilmenite magnetism at low *T*.

cone, such that the angle between the **c**-direction and the tilt cone is $\gamma > 90°$.

For given angles θ, ϕ, there is a unique direction $\mathbf{L}(\theta, \phi, \gamma)$ on the tilt cone that lies closest to the paleofield direction $(0,0,1)$. This direction is

$$
\mathbf{L}(\theta, \phi, \gamma) = \begin{pmatrix} \cos\gamma \sin\theta \cos\phi - \sin\gamma \cos\theta \cos\phi \\ \cos\gamma \sin\theta \sin\phi - \sin\gamma \cos\theta \sin\phi \\ \cos\gamma \cos\theta + \sin\gamma \sin\theta \end{pmatrix}.
$$

The general direction of an arbitrary lamellar moment that lies on the cone defined by the opening angle γ allows for an additional rotation $\beta \in [0, 2\pi[$ around the **c**-axis.

Average NRM as a function of tilt angle γ

A lamella with *c*-direction (θ, ϕ) has the closest lamellar moment to the field direction $\mathbf{e}_z$ in direction $\mathbf{L}(\theta, \phi, \gamma)$. The field component that influences the orientation of this lamellar moment is therefore $\mathbf{L}(\theta, \phi, \gamma) \cdot \mathbf{e}_z$. At the same time the component this lamellar direction contributes to the total NRM is also $\mathbf{L}(\theta, \phi, \gamma) \cdot \mathbf{e}_z$. Accordingly, after averaging over the sphere of all possible directions where the probability to encounter the *c*-direction (θ, ϕ) is denoted

as $p(\theta, \phi)$, yields

$$
NRM(\gamma) := \int_{\theta=0}^{\pi} \int_{\phi=0}^{2\pi} (\cos\gamma \cos\theta + \sin\gamma \sin\theta)^2
$$
$$
p(\theta, \phi) \sin\theta \, d\theta \, d\phi.
$$

If the *c*-axes are equally distributed over the unit sphere with area 4π, the density is constant, $p(\theta, \phi) = \frac{1}{4\pi}$ and

$$
NRM(\gamma) = \frac{1}{2} - \frac{1}{6} \cos 2\gamma.
$$

If the lamellar moments are not chosen optimally on the cone, but randomly distributed with a variable rotation angle β around the *c*-axis, the NRM intensity as a function of θ averaged over β is

$$
NRM(\gamma, \theta) = \frac{1}{2\pi} \int_{\beta=0}^{2\pi} (\cos\gamma \sin\beta \cos\theta + \sin\gamma \sin\theta)^2 \, d\beta
$$
$$
= \frac{1}{8} (3 - \cos 2\theta + \cos 2\gamma (3\cos 2\theta - 1)).
$$

Integrating this over a constant density on the sphere leads to the smaller NRM estimate
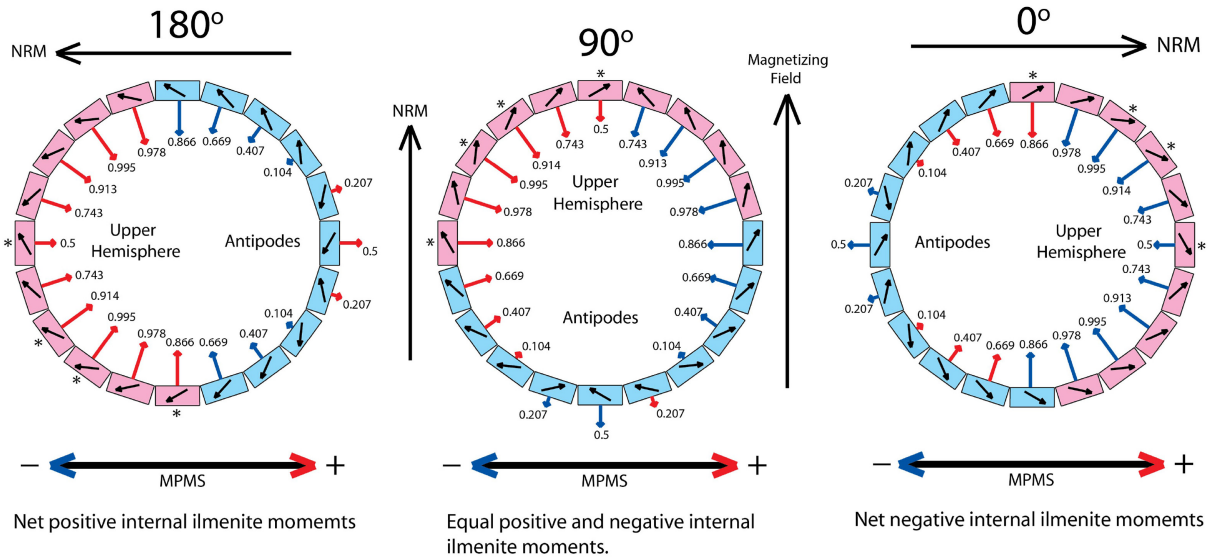
$$
NRM(\gamma) = \frac{5}{12} - \frac{1}{4} \cos 2\gamma.
$$

Figure A3. Centre: Circular 2-D cross-section through a randomly oriented spherical array. This particular array shows twenty exsolved titanohematite plates parallel to (001) with c axes of the plates oriented at 18° intervals from the MPMS axis, at 180°, 162°, ..., 18°, 0°. A crystal with c-axis at 0° is thus oriented 90° from the natural magnetizing field (upper asterisk). Because the hematite sublattice magnetizations (black arrows) are tilted 30° out of the (001) plane, there are two sets of such plates, the upper hemisphere set (pink) with the subattice magnetizations closer to the magnetizing field orientation, and the antipodes set (light blue) with the sublattice magnetizations further from the magnetizing field. The exception to this are the plates at 0° and 90°, where plates in both sets have sublattice magnetizations at the same angle to the field. In this figure the resulting relative theoretical ilmenite magnetizations for these plates at low T, caused by antiferromagnetic coupling to the lamellar moments, will be proportional to the sine of their angle to the magnetizing field, consistently equal or larger in the upper hemisphere set than in the antipodes set. In the 90° orientation with the NRM oriented 90° to the MPMS field, one can see that the positive and negative ilmenite moments are exactly equal. Left and right: Illustration of the consequences of 90° rotation of the array in center to either 0° (right) or 180° (left). As the NRM is rotated clockwise from 90° towards 0°, ilmenite moments oriented negatively to the MPMS will increase, but even at 0° most of those in the blue antipodes set point positively. As the NRM is rotated counterclockwise from 90° towards 180°, ilmenite moments oriented positively to the MPMS will increase, but even at 180° most of those in the blue antipodes set point negatively. These features agree with experimental results, both in relations between 300 K lamellar moments and low-T exchange bias, and the fact that no sample shows complete dominance of negative or positive exchange bias as a result of ilmenite magnetization.
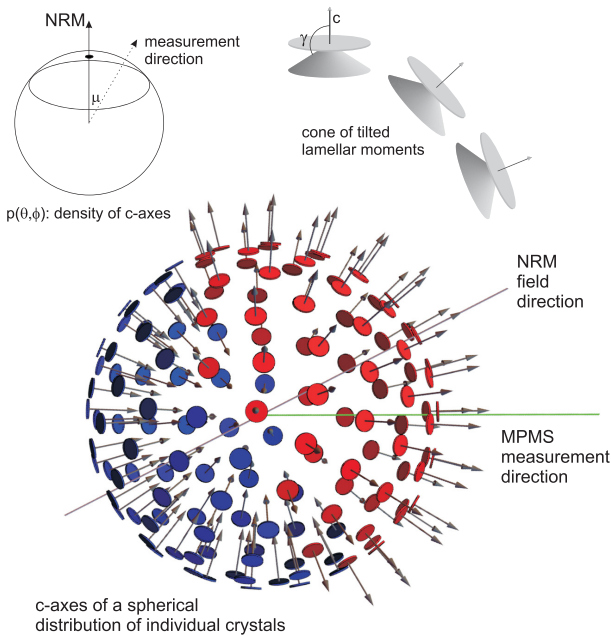
For each lamella with c-axis orientation (θ, ϕ), the ilmenite moment that orders below $T_N = 57$ °C will point along the c-axis in the direction $\mathbf{e}(\theta, \phi)$ opposite to the tilted hematite moment.

Figure A4. Geometric sketch of the factors influencing the averaged NRM of a population of nanoscale ilmenite lamellae in equidistributed randomly oriented hematite hosts.